INTERNATIONAL ATOMIC ENERGY AGENCY
UNITED NATIONS EDUCATIONAL, SCIENTIFIC AND CULTURAL ORGANIZATION

INTERNATIONAL CENTRE FOR THEORETICAL PHYSICS
34100 TRIESTE (ITALY) - P.O.B. 586 - MIRAMARE - STRADA COSTIERA 11 - TELEPHONES: 224281/2/3/4/5/6
CABLE: CENTRATOM - TELEX 460392-1

SMR/111 - 11

SECOND SUMMER COLLEGE IN BIOPHYSICS

30 July - 7 September 1984

I. Small angle X-ray diffraction and scattering
II. X-ray diffraction from muscle

A.R. FARUQI
Laboratory of Molecular Biology
Medical Research Council
University Medical School
Hills Road
Cambridge CB2 2QH
U.K.

Part 1

Lecture Notes on Small Angle X-ray Diffraction and Scattering
Prepared for Biophysics Summer College, Trieste, August 1984.

A.R. Faruqi, M.R.C. Laboratory of Molecular Biology,
Cambridge, U.K.

Introduction

To understand the fundamental principles of X-ray scattering, it is instructive to remind ourselves how visible radiation is used in image formation within a microscope. According to Abbe's theory of image formation the object acts as a secondary scatterer of light, part of which may be collected by a lens as shown in Fig.1. Light scattered at the same angle is brought together at the same point in the focal plane, and the interference of waves arising from different parts of the object produces a diffraction pattern in the focal plane. Each point in the focal plane may be treated as a source of coherent secondary waves which interfere with each other to form the final image.

If a parallel beam of monochromatic light illuminates a slit with a lens placed behind it the diffraction pattern of the slit is generated due to interference between waves originating at various points in the slit as shown in Fig.2. If the width of the slit is a, then the intensity in the imaging plane is given by

$$I = R^2 = R_o^2 \frac{\sin^2 \beta}{\beta}$$

where

$$R_o = Ka$$

$$\beta = \pi a \sin\theta / \lambda$$

where K is a constant for a given geometry and θ is the scattering angle. The shape of the intensity curve is shown in the Fig.3. There is a maxima at $\beta = 0$ (where $\sin \beta = 1$) followed by subsidiary maxima. The minima occur at π, 2π ... etc.

Wave Motion

A wave propagating along the x-axis, as shown in Fig.4, may be described by:

$$y = a \sin (wt - kx)$$

where a = amplitude

$$\omega = \frac{2\pi}{T}$$

T = period

$k = \frac{2\pi}{\lambda}$ (λ = wavelength)

The quantity (wt-kx) is the phase of the wave and is important in finding the sum of two waves. The phase difference corresponding to distance λ is 2π so that for an arbitrary distance δx it is $\frac{2\pi}{\lambda}\delta x$. A more convenient representation for waves is

$$y = a \exp i(wt-kx)$$

$$= A \exp iwt \qquad \text{where } A = ae^{-ikx}$$

the intensity is given by

$$I = AA^* = |A|^2 = a^2$$ the square of the amplitude.

Scattering Geometry (based mainly on Cantor & Schimmel)

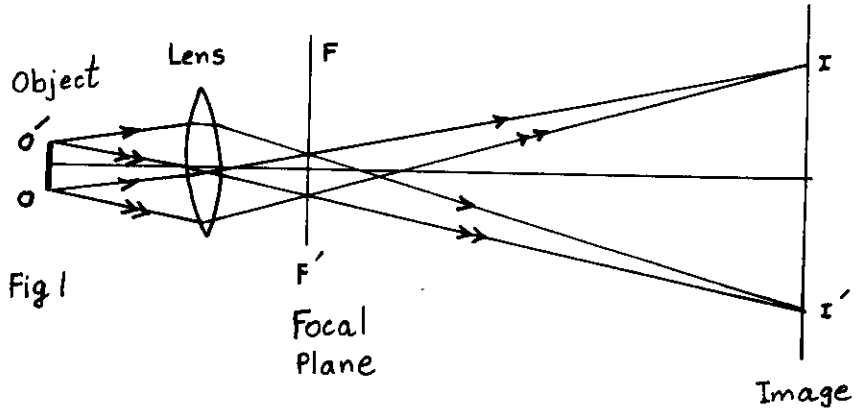

Fig 1

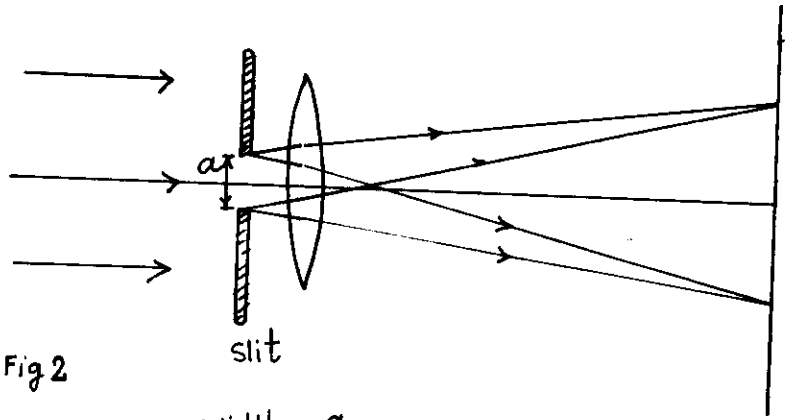

Fig 2

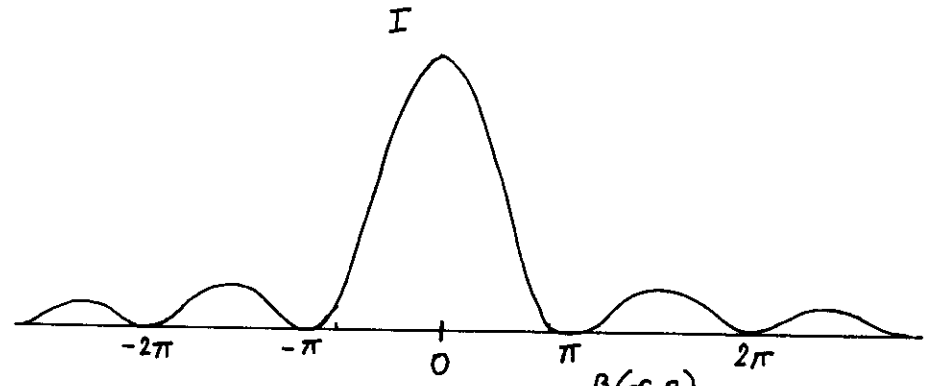

Fig 3

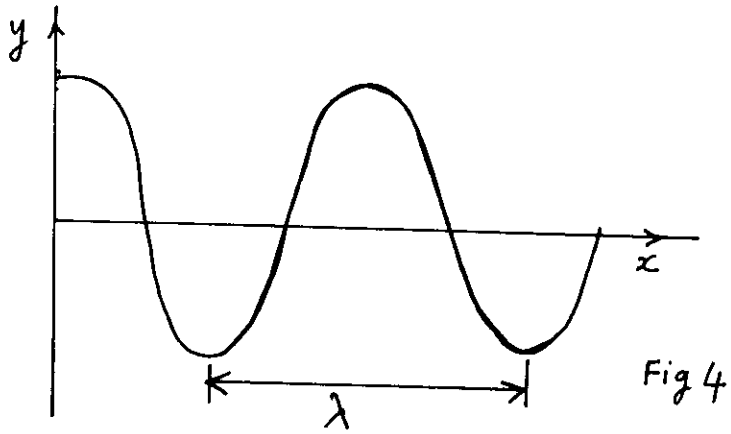

Fig 4

The simplest geometry of an X-ray scattering system consists of a collimated beam of X-rays impinging on a sample consisting of a single electron at the origin. The incident beam is described by a unit vector $\hat{S}_o$ and the scattered beam along 2θ by $\hat{S}$ as shown in Fig.5. As we are only interested in elastic scattering of the X-rays the wavelength does not change. It is mathematically convenient to define a new scattering vector $\underline{S}$:

$$\underline{S} = \hat{S}/\lambda - \hat{S}_o/\lambda$$

The value of $\underline{S}$ can vary between 0 and 2 having dimensions of reciprocal distance in a system called reciprocal space.

Suppose now that we move the electron away from the origin and ask how the scattering changes. The structure factor, $F(\underline{S})$ is defined as the ratio of the radiation scattered by any real sample to that scattered by a single electron at the origin. We place a single electron at position $\underline{r}$ as shown in Fig.6. The scattering angle is the same (approximately) but the path difference is

$$(\hat{S} - \hat{S}_o).\underline{r}$$

i.e. the phase difference will be

$$2\pi/\lambda\,(\hat{S}-\hat{S}_o).\underline{r} = 2\pi\underline{S}.\underline{r}$$

Therefore if the radiation scattered at the origin is $E(\underline{S})$, then moving the electron to $\underline{r}$ simply causes a phase shift and the scattered radiation is $E(\underline{S})\exp(2\pi i\underline{S}.\underline{r})$. The structure factor is $\exp(2\pi i\underline{S}.\underline{r})$

In general because electrons are not localised, we define an electron density $P(\underline{r})$ in a volume element $d\underline{r}$ located at $\underline{r}$. the scattering is then proportional to $P(\underline{r})\,d\underline{r}$ which is simply the number of electrons in the volume element $d\underline{r}$. For continuous electron density at r, the structure factor is

$$F(\underline{S}) = \int P(\underline{r}) \exp(2\pi i\,\underline{S}.\underline{r})\,d\underline{r} \qquad (6)$$

A sample with many discrete scattering sites has a structure factor which is a sum of (6) for all values of r.

$$F(\underline{S}) = \int d\underline{r}\; P(\underline{r}) \exp(2\pi i\underline{S}.\underline{r}) \qquad (7)$$

This is one of the most important equations in X-ray scattering and crystallography allowing one to calculate the amount of scattering from a knowledge of the electron density distribution.

The mathematical form of (7) is equivalent to a Fourier Transform. The physical meaning is that the structure factor is the Fourier Transform of the object.

As $F(\underline{S})$ is the Fourier Transform of $P(\underline{r})$, the inverse must hold as well

$$P(r) = \frac{1}{V}\int d\underline{S}\; \exp(-2\pi i\,\underline{S}.\underline{r})\,F(\underline{S}) \qquad (8)$$

taken over all reciprocal space.

Equations (7) and (8) allow one to intercovert structure factors and electron densities, providing each is known over all space.

Structure Factor

The structure factor is a complex number

$$F = |F|\exp(i\varphi) \qquad (9)$$

or

$$F = F_r + iF_i \qquad (10)$$

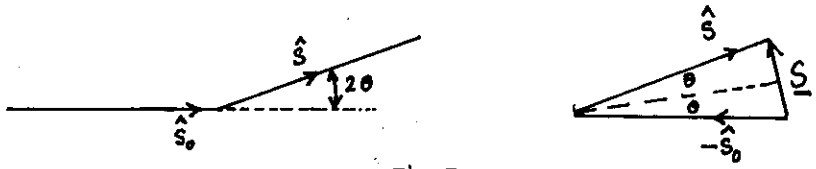

Fig 5

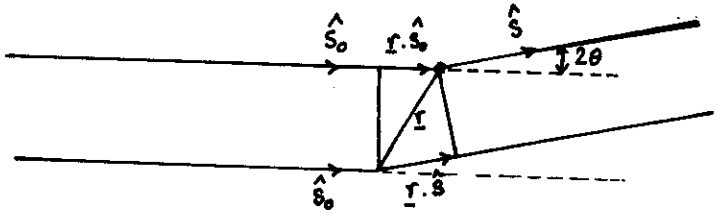

Fig 6

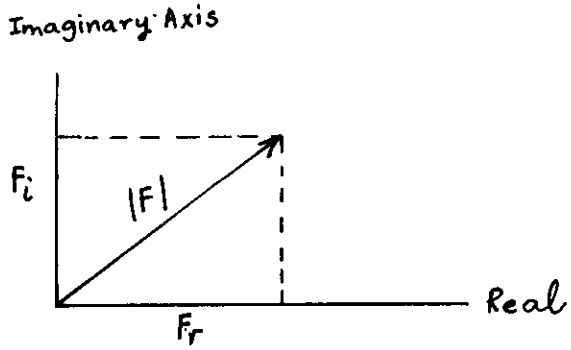

Fig 7

$|F|$ is known as the amplitude of the Structure factor F and $\exp(i\varphi)$ as the phase.

$$F_r = |F| \cos\varphi$$

$$F_i = |F| \sin\varphi \qquad (11)$$

$$|F| = (F_r^2 + F_i^2)^{\frac{1}{2}}$$

$$= \tan^{-1} F_i/F_r$$

Experimentally, one observes only the intensity scattered at an angle 2θ, given by

$$I(\underline{S}) = F(\underline{S})\, F^*(\underline{S}) = |F|^2$$

The intensity is real so instead of squaring F(S) we multiply it by its complex conjugate to get a real number. Unfortunately there is no simple way of getting φ (phase angle) and this has to be estimated or obtained indirectly.

Substituting (10) in (8)

$$P(r) = \int [F_r(\underline{S}) + i\, F_i(\underline{S})]\, e^{-2\pi i \underline{S}.\underline{r}} d\underline{S}$$

$$P^*(r) = [F_r(\underline{S}) - i\, F_i(\underline{S})]\, e^{+2\pi i \underline{S}.\underline{r}} d\underline{S}$$

As the density is real $P(r) = P^*(r)$ for any value of r

i.e. $F_r(S) = F_r(-S)$

$$F_i(S) = -F_i(-S)$$

i.e. the real part is symmetric about the origin of reciprocal space ($S = 0$) whereas the imaginary part is antisymmetrical, i.e. $F(\underline{S})$ is a conjugate function

$$I(S) = |F(S)|^2$$

$$= F_r^2 + F_i^2$$

$$= |F(-\underline{S})|^2$$

$$= I(-S) \qquad (12)$$

i.e. the intensity is symmetric about the origin, known as Friedels Law.

Scattering from atom at origin

The atom can be assumed to be spherically symmetric, i.e.

$P(\underline{r}) = P(r)$

Eqn (7) is

$$F(S) = \int dr P(\underline{r}) \exp(2\pi i \underline{S}.\underline{r}) \qquad (7)$$

$$= \int d\varphi \int \sin\theta\, d\theta \int dr P(r)\, r^2 \exp(2\pi i r.S)$$

$$= 2\pi \int dr P(r) r^2 \int_0^{\pi} d\theta\, \sin\theta\, (2\pi i r S \cos) \qquad (13)$$

If $x = \cos\theta$

$$F(S) = 4\pi \int dr P(r) r^2 \left[\frac{\sin 2\pi r S}{2\pi r S}\right] f(S) \qquad (14)$$

where f(S) is the atomic scattering factor

For real atoms $P(r) = ZNe^{-kr}$

where Z = no of electrons and N is a constant. Eqn 14 can be integrated to give

$$f(S) = ze^{-\frac{\pi^2 S^2}{k}} \quad (15)$$

For forward scattering, i.e. S = 0, f(S) is simply equal to the number of electrons, but the scattering factor drops sharply for increasing angle.

If the atom was centred at r_n instead of the origin, the scattering would be given by

$$F(S) = f(S) \exp(2\pi i \underline{S}.\underline{r}_n) \quad (16)$$

and for a set of N atoms, each located at r_n with scattering factor fn, the structure factor is

$$F(S) = \sum_{n=1}^{N} fn(S)\exp(2\pi i \underline{S}.\underline{r}_n) \quad (17)$$

If the N atoms belong to a molecule, then (17) represents a molecular structure factor Fm(S).

The Interference Function

As mentioned earlier, the phase shift introduced by an atom at r_n is $\exp(2\pi i \underline{S}.\underline{r}_n)$; if there are two atoms, one at the origin and the other at r_n, the structure factor is

$$F(\underline{S}) = f(S)\ (1 + \exp(2\pi\ i\underline{S}.\underline{r}_n) \quad (18)$$

$$I(S) = f^2(S)\ (1 + \exp(2\pi\ i\underline{S}.\underline{r}_n)\ (1 + \exp(-2\pi\ i\underline{S}.\underline{r}_n)$$

$$I(S) = 2f^2(S)\ [\ 1 + \cos(2\pi\underline{S}.\underline{r}_n)] \quad (19)$$

The intensity of the scattered radiation consists of two terms: an individual atom term $f^2(S)$ and an interference function $\cos(2\pi\underline{S}.\underline{r}_n)$ producing fringes similar to those seen in two slit experiments.

Consider an atom at the origin, situated within the array will give a structure factor

$$F_n(\underline{S}) = \exp(2\pi\ in\underline{S}.\underline{a})f(S) \quad (20)$$

and the structure factor for the whole array

$$F_{tot}(S) = f(S) \sum_{n=-N}^{+N} \exp(2\pi\ in\underline{S}.\underline{a}) \quad (21)$$

The scattering from a linear array of molecules would be given by a similar function to that given in (20) with f(S) replaced by Fm(S)

Summing the series in equation (21)

$$Ftot(S) = f(S)\ \frac{\mathrm{Sin}[(2n+1)\pi\underline{S}.\underline{a}]}{\mathrm{Sin}(\pi\underline{S}.\underline{a})} \quad (22)$$

$$I_{tot}(S) = |F_{tot}(\underline{S})|^2 = [f(S)]^2\left\{\frac{\mathrm{Sin}[(2n+1)\pi\underline{S}.\underline{a}]}{\mathrm{Sin}\ (\pi\underline{S}.\underline{a})}\right\}^2 \quad (23)$$

As N becomes large, the intensity tends to 0 everywhere except where $\underline{s}.\underline{a}$ is integral.

In the limit where $\underline{s}.\underline{a}$=0, the quotient in eqn (22) tends to 2N+1, i.e. the structure factor is enormous each time Sin $(\pi\underline{s}.\underline{a})\to 0$ which happens every time $\underline{s}.\underline{a}$. is an integer. This is known as the Von Laue condition:

$$\underline{S}.\underline{a}. = h \quad h=0, +1, +2, \text{ etc.} \quad (24)$$

only when this condition is satisfied will any scattering be observed. If $\underline{S}$ is a vector in a plane perpendicular to $\underline{a}$ then $\underline{S}.\underline{a} = 0$. If $\underline{s}.\underline{a} = 1$ then $\underline{S}$ is a vector from the origin to a plane perpendicular to $\underline{a}$ and spaced $1/a$ away. Extending the argument, it is clear that (24) defines a series of parallel planes with spacing $1/a$ which define all values of the scattering vector which produce a measurable intensity.

The direction of $\hat{S}_o$ puts more restrictions on the scattering vector $\underline{S}$. The length of the vector along $\hat{S}$ is always $1/\lambda$, the end of $\underline{S}$ defines a sphere of radius $1/\lambda$ centred as shown in Fig.10, known as the sphere of reflection. Scattering is only observed if the scattering vector lie on points formed by the intersection of the surface of sphere and a set of parallel planes.

Scattering takes place at the intersection of the plane $\underline{S}.\underline{a} = h$ with the sphere of reflection. The scattering angle α is given by : $\sin\alpha = \frac{h\lambda}{a}$

As the maximum value of $\sin\alpha$ is 1, if a is 5Å and λ is 1Å, the maximum value of h is a; the layer lines are given by $-5<h<5$ and the pattern will have 11 layer lines.

It is mathematically simple to extend this scheme to diffraction from three dimensional crystals. The scattering only occurs when the Von Laue condition is satisfied for periodicities in all three directions, viz

$\underline{S}.\underline{a} = h$
$\underline{S}.\underline{b} = k$
$\underline{S}.\underline{c} = l$

This results in a three dimensional lattice of points with a spacing of 1 perpendicular to $\underline{a}$, $1/b$ perpendicular to $\underline{b}$ and $1/c$ perpendicular to $\underline{c}$. Diffraction only occurs when $\underline{S}$ intersects one of the lattice points which, for obvious reasons is called the reciprocal lattice and the space it occupies reciprocal space. The lattice spacings are a*, b* and c*.

In our discussion above we have assumed one atom per lattice point. The positions of the atoms define a set of cells bounded by $\underline{a}$, $\underline{b}$ and $\underline{c}$
A vector drawn from the origin to the jth atom position is

$\underline{r} = x\underline{a} + y\underline{b} + z\underline{c}$

as atoms lie at the corner of cells x,y and z are integers

The structure factor, extending (20) is

$$Ftot(\underline{S}) = \sum_x \sum_y \sum_z f(S) \exp(2\pi i \underline{S}.(x\underline{a} + y\underline{b} + z\underline{c}) \quad (25)$$

$$Ftot(h,k,l) = \sum_x \sum_y \sum_z f(S) \exp(2\pi i(hx + ky + lz) \quad (26)$$

where h, k and l are integers. As in eqn (8) we can invert the Fourier series to obtain electron density

$$\rho(x,y,z) = \frac{1}{NV} \sum_{h=-\infty}^{\infty} \sum_{k=-\infty}^{\infty} \sum_{l=-\infty}^{\infty} F_{tot}(hkl)\exp(-2\pi i(hx + ky + lz)) \quad (27)$$

where V = volume of the unit cell = $\underline{a}.\underline{b} \times \underline{c}$ and NV = volume of the entire array. The dimension of F(h,k,l) is number of electrons and P(x,y,z) number of electrons per unit volume.

Very similar equations hold for any real crystal where the repeating unit is a unit cell. Again, as shown above, each unit cell is defined by three vectors $\underline{a}$,$\underline{b}$ and $\underline{c}$. The contents of the unit cell may be very different in the sense that it might consist of a molecule or several molecules. The sampling of the structure factor is restricted to the reciprocal lattice, but it is the molecular structure factor which is sampled this time.

The position of the jth atom in the unit cell is

$\underline{r}_j = x_j\underline{a} + y_j\underline{b} + z_j\underline{c}$

(9)

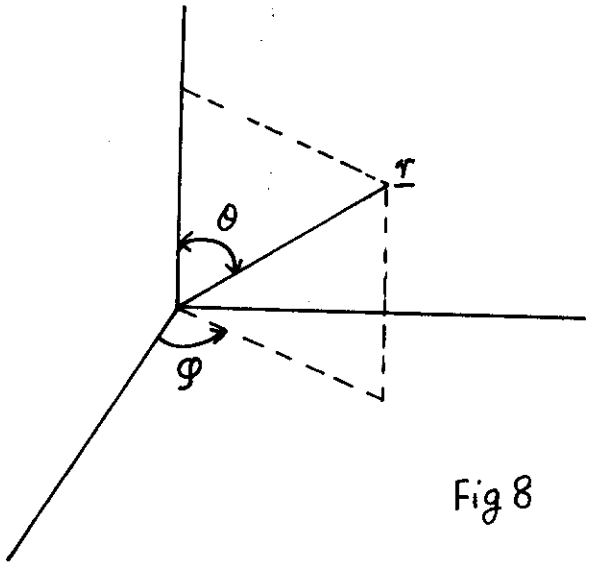

Fig 8

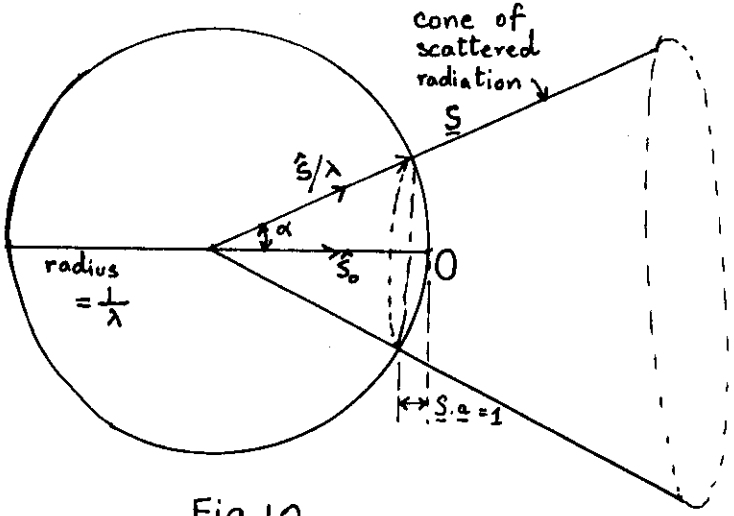

Fig 10.

(10)

where x_j, y_j and z_j are now fractions of the unit cell dimensions. The structure factor is given by

$$F_m(h,k,l) = \sum_j f_j(S)\exp 2\pi i(hx_j + ky_j + lz_j) \qquad (28)$$

This is an important equation because it allows the structure of a crystal (or its electron density) to be solved from a knowledge of the structure factors.

Solution Scattering

In a large number of cases, it is not possible to make single crystals of a macromolecule and carry out structure determination. It is nevertheless possible to obtain structural information, albeit with much lower resolution by studying the scattering produced by the macromolecule in dilute solution.

Assuming that intermolecular interference effects are negligible, the scattering by one molecule is simply the molecular structure factor (similar to (17))

$$F_m(\underline{S}) = \sum_{n=1}^{N} f_n(S)\exp(2\pi i \underline{S}.\underline{r}n) \qquad (29)$$

the sum being over all N atoms in the molecule.

$$I(\underline{S}) = F_m F_m^* = f_e^2(S)\sum_{n=1}^{n_e}\sum_{m=1}^{n_e}\exp\left(2\pi i\,\underline{S}\cdot\underline{r}_{nm}\right) \qquad \cdots(30)$$

In practice it is sufficient to have the scattering particles in a dilute solution so that there is no correlation between the positions of the particle and the scattering intensities are simply added. There is some contribution from the solvent which can be subtracted out.

where n_e = no. of electrons in the molecule

$r_{nm} = r_n - r_m$ the vector between electrons n and m.

$f_o(S)$ = scattering factor for a single electron

For any measurement carried over a period of time the molecule will assume all possible orientations: In a large assembly of molecules, all orientations will be present at one time.

$$\langle I(S)\rangle = f_o^2(S)\sum_{n=1}^{n_e}\sum_{m=1}^{n_e}\int d\Omega\,\exp\left(2\pi i\,\underline{S}\cdot\underline{r}_{nm}\right) \qquad (31)$$

integrated over all possible relative orientations of $\underline{r}_{nm}$ and $\underline{S}$

$$\langle I(S)\rangle = 4\pi f_o^2(S)\sum_{n=1}^{n_e}\sum_{m=1}^{n_e}\frac{\sin 2\pi S r_{nm}}{2\pi S r_{nm}} \qquad (32)$$

Debye Formula

The scattering only depends on 2θ and not the orientation of $\underline{S}$; this is understandable because the speciment itself has no preferred orientation in space.

For scattering at very small angles $\theta \to 0$ $S = \frac{2\sin\theta}{\lambda}$ also $\to 0$. Using the expansion for Sinx

$$\lim_{x\to 0}\frac{\sin x}{x} = 1 - \frac{x^2}{6} + [0]$$

$$\langle I(S)\rangle = 4\pi f_o^2(0)\sum_{n=1}^{n_e}\sum_{m=1}^{n_e}\left[1 - \frac{(2\pi S r_{nm})^2}{6}\right] \qquad \cdots(33)$$

It is convenient to define a parameter known as the radius of gyration of the molecule (Rg). By analogy with classical mechanics, Rg can be considered as the electronic radius of gyration of the particle about its electronic centre of mass. It is the 'spatial extent' of the molecule and

gives indiciations regarding its shape. It is can be shown that the radius of gyration of a complex unit consisting of (n+1) identical units is given by

$$R_g^2 = \frac{1}{(n+1)^2} \Sigma r^2_{ij}$$

where r_{ij} is the distance between residues i and j. If one imagines the macromolecule to be a complex unit of ne identical units

$$Rg^2 = \frac{1}{ne^2} \Sigma r_{nm}^2 = \frac{1}{2ne^2} \Sigma\Sigma_{n\ m} r^2_{nm} \qquad (34)$$

$$\text{or} \quad \Sigma\Sigma_{n\ m} r_{nm}^2 = 2ne^2Rg^2 \qquad (35)$$

Substituting this in (33)

$$\langle I(S) \rangle = 4\pi fo^2(0)ne^2 \left(1 - \frac{4\pi^2S^2Rg^2}{3}\right) \qquad (36)$$

If we divide the scattered intensity by $4\pi fo^2(0)$, we get the intensity scattered by the macromolecule relative to a single electron at the origin. Also putting $\frac{2\sin\theta}{\lambda}$ for S

$$\langle I(\theta) \rangle = ne^2 \left(1 - \frac{16\pi^2Rg^2\sin\theta}{3\lambda^2}\right) \qquad (37)$$

$$\log\left[\frac{I(\theta)}{I(o)}\right] = -\frac{\left(\frac{4\pi R_g \sin\theta}{\lambda}\right)^2}{3} \qquad (38)$$

$$\log I(\theta) = \log I(0) - K R_g^2 (2\theta)^2 \qquad (39)$$

This expression shows that, at small angles, scattering is proportional to the square of the number of electrons or to the square of the molecular weight. A plot of intensity against $\sin\theta$ gives the radius of gyration.

Equ (37) can be re-arranged by noting that for small x, $\exp(-x^2/a) = 1 - \frac{x^2}{a}$ This is known as a Guinier Plot where K is a constant. If a plot is made of the scattered intensity as a function of the square of the scattering angle and plotted in a logarithmic fashion, the slope of the very small angle region gives the radius of gyration.

If molecules with the same volume possess different anisotropies, this is reflected in the value of Rg; the greater the anisotropy, the higher the value of Rg. In some cases the measurement of Rg will also yield information on conformational changes in the molecule.

The intensity of scattering given by (38) is only valid if there is no phase relation between waves scattered by separate molecules, i.e. there is no inter-particle interference phenomena. To eliminate any possibility of this happening it is customary to dilute the concentration in a whole series of experiments and extrapolate to zero concentration.

A molecule in solution is not comparable with one in a gas because of the interaction of the various charged groups which interact with the polar solvent molecules and any ions that may be present in the solution. This effect is particularly strong with nucleic acids which have negative phosphate groups on their surface. The specimen under study is therefore surrounded by an ion and water shell which affects the measurement of the radius of gyration.

For long, rod-like scattering material in which one axis is considerably longer than the other two axes, it is possible to separate the scattering into 'length' and 'cross-section' components, and by suitable re-arrangement the 'length' contribution is eliminated. This is useful in studying the radius of gyration of the cross-section under various

experimental conditions. For instance the radius of gyration of DNA was measured in solution in the presence of NaCl and CsCl and it was found that in cross-section, DNA consists of a cylindrical core of high density surrounded by a shell of much lower density to a radius of 10Å.

Wider-Angle Scattering

As discussed above we can obtain the radius of gyration of a particle by studying scattering at small angles. However, the information is available also at wider angles which can be extremely useful. The shape of the scattering curves can be compared to what is expected from standard models, such as solid uniform ellipsoids of revolution and information about the general shape.

It is instructive to work out the scattering expected from the simplest structure, viz a sphere of radius R and having a uniform electron density So. The expression is very similar to that for scattering from a single atom at the origin which was presented in equation (14) which was the accompanying plot. The positions of the maxima in the scattered intensity give the radius.

Fibre Diffraction (based mainly on Holmes & Blow)

Many biological molecules are long and threadlike or fibrous by nature and others can be oriented by various techniques to form fibres. The fibres have a common axis along their length but their orientation about the long axis is random. In many cases the arrangement of atoms follows a helical path along the fibre axis and X-ray diffraction picks out the regularity in the arrangement of these atoms. At the same time, non-regular parts of the structure simply generate extra background.

Certain forms of DNA form micro-crystals which have a common axis but are oriented at random around it. This is equivalent to having a micro-crystal which was rotated around the common axis during an experiment. The fibre diagram is therefore equivalent to a rotation diagram.

Most biological fibres are only capable of forming semi-crystalline structures and an example illustrates the difference between crystalline and semi-crystalline packing. Consider a pile of pencils which will pack together to form a hexagonal array. If all the pencils were pointing in the same direction and the writing was at the same height this would be one layer of a three dimensional lattice of pencils. However, as is more likely, if the writing is randomly oriented and the height of the pencil is staggered then we have a pseudo-hexagonal array of pencils.

The 'disorder' in the lattice produces sampling of the molecular transform only at low resolution, i.e. at small angles of scattering. At low resolution the more detailed features of the structure are not in evidence, and to consider our example of the pencil stack, it does not matter that the pencils are at different height or that they are randomly oriented because all that will be evident is a rod of uniform density.

As the fibre has regular repeats along its length it acts almost as a grating which gives rise to various orders of diffraction recorded as "layer lines". The zero-order layer line is known as the equator and the line at right angles to this as the meridian.

Crystalline fibres have a common axial direction but individual micro-crystals are oriented at random angles to this common direction. An X-ray measurement 'samples' the crystals at all orientations. Using the convolution theorum, the scattering from a microcystal may be written as

$$F_{Tot} = F_m(\underline{S})\, F_L(\underline{S}) \qquad (41)$$

where $F_m(\underline{S})$ is the molecular structure factor, and
$F_L(\underline{S})$ is the sampling function generated by the lattice, being the Fourier transform of the lattice.

The scattered intensity in the fibre pattern is given by

$I = \langle |F_{Tot}|^2 \rangle$ rotationally averaged about the common axis

and, more formally

$$I = \langle |F_m(\underline{S})\, F_L(\underline{S})|^2 \rangle \qquad (42)$$

the angle brackets mean that the terms inside have to be averaged over the various types of inherent disorder.

For non-crystalline fibres there is no regular lattice and the intensity is

$$I = \langle |F_m(\underline{S})|^2 \rangle \qquad (43)$$

averaged over molecular orientations. This is similar to solution scattering equations.

Scattering form a Helix

In its simplest form a helical molecule consists of an atom arranged periodically along a helix, successive atoms being related by a screw axis of symmetry.

By analogy with equation (21), the structure factor for the helical molecule may be written as

$$F_{Tot}(\underline{S}) = f(\underline{S})\, F_l(\underline{S}) \qquad (44)$$

where f(S) is the atomic scattering factor of the atom and $F_1(S)$ is the sampling function of the lattice, $F_l(S)$ being the fourier transform of the lattice.

The helical lattice can be generated by taking the product of a helical line with a set of planes each plane representing the position of a single residue. The Fourier transform of a product is equal to the convolution of the Fourier transforms of the two components and the sampling function of the helical point lattice is, simply $F_l = F_c\, F_u$ where F_c and F_u are respectively the Fourier transform of a helical line and a set of planes.

If we were to now replace a group of atoms for each lattice point with F_R as the structure factor, the total structure factor for the helix will become

$$F_{Tot} = F_R\, F_l \qquad (45)$$

It is more convenient to use cylindrical polar coordinates to describe helical molecules than Cartesian coordinates. We use x,y,z and r,ϕ,z as the Cartesian and polar coordinates in real space and x,y,z and R,θ,Z in reciprocal space.

As we are imposing cylindrical symmetry in the scattering it is again more convenient to analyze the scattered waes with cylindrical symmetry.

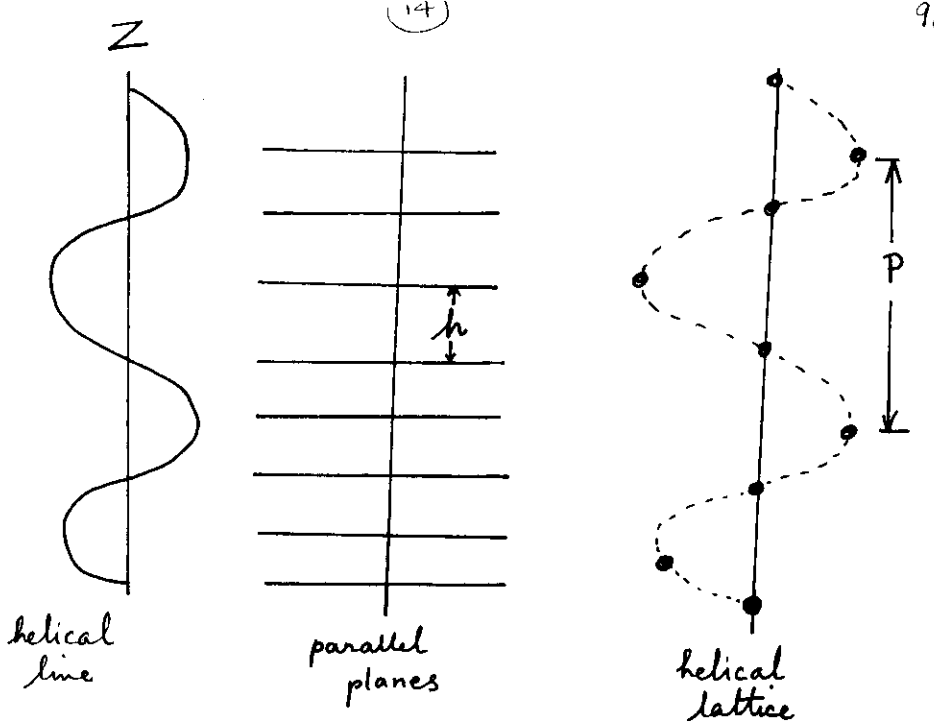

Fig 11

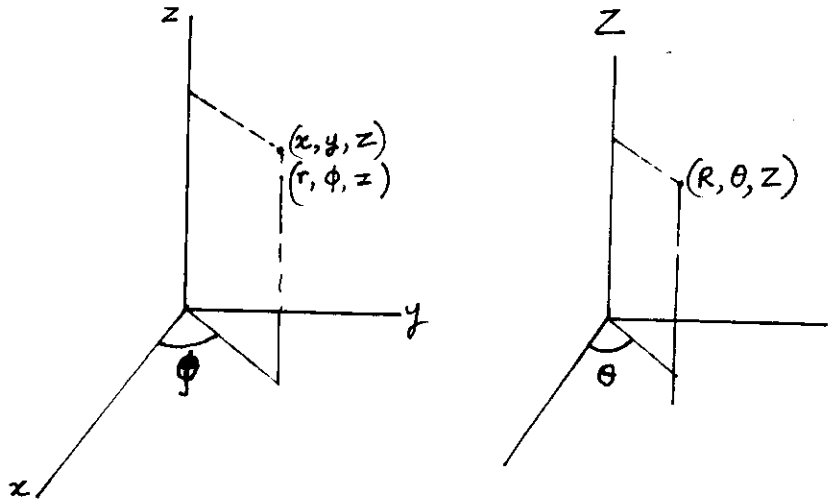

Fig 12

The simplest wave with cylindrical symmetry is a zero order Bessel function (Jo) which is like a ripple spreading out in a pond. This type of wave only varies with radius and not along the azimuth. The more general cylindrical wave will vary sinusoidally in azimuth containing an integral number of wavelengths in one rotation. A cylindrical wave of order n may be written down as

$$C_n(r,\varphi) = J_n(2\pi Rr)\cos n\left(\varphi - \theta + \frac{\pi}{2}\right) \quad \cdots (46)$$

where Jn (2 Rr) is a Bessel Function of order n,

n denotes the number of oscillations in the azimuth

R is analogous to wave number, specifies radial oscillation

specifies orientation of the wave

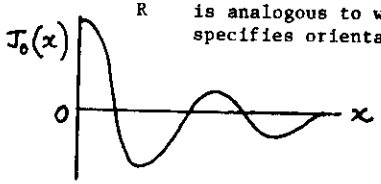

Jo (x), shown on the left, starts at a maximum and dies like an attenuated sine wave. All other Bessel functions are at the origin, rise to a peak at approximately x=n and then oscillate like Jo(x).

Just as any function can be analysed in terms of plane waves, it can also be analyzed in terms of cylindrical waves. The building of an electron density model from the knowledge of how much each of the cylindrical waves is present is called Fourier-Bessel synthesis and it requires a Fourier transformation in cylindrical coordinates.

The transform of some simple object are described.

(1) A ring of wire, radius r_o

Jo ($2\pi Rro$)

(2) For a ring in which the density fluctuates sinusoidally n times around the ring, the transform is:

$2ni^n$ Jn ($2\pi Rr_o$) Cos n θ

which is a cylindrical wave, i.e. we can associate a ring of density fluctuating sinusoidally with a cylindrical wave of the same frequency.

Fourier Transform of a Helix

Consider a helix consisting of single atoms for simplicity. There are four parameters which specify the helix:

r_o radius of the helix

c distance in which the structure repeats exactly along the z-axis

t number of turns in one repeat distance c

u number of atoms in one repeat distance c.

P , the pitch is given by $\frac{c}{t}$. It was shown by Cochran, Crick and Vand that the Fourier Transform of the helix is

$$F\left(R,\theta,\frac{l}{c}\right) = \sum_n f J_n(2\pi Rr_0)\exp i\left[n\left(\theta - \varphi + \frac{\pi}{2}\right) + \frac{2\pi lz}{c}\right] \quad \cdots (47)$$

The Z coordinate is replaced by c because as the structure has period c the transform can only be non-zero at integral multiples of c. The integer l is known as the layer line number. The equation contains cylindrical waves due to the Beasel Function. f is the scattering factor of the atom.

There is a selection rule imposed on the values of l given by

$l = tn + um$

where m is also an integer from $-\infty$ to $+\infty$, but in practice only values close to zero are important.

Almost any helical molecule will consist of many different types of atoms and the transform is given by:

$$F\left(R,\theta,\frac{l}{c}\right) = \sum_n \sum_j f_j J_n(2\pi Rr_j)\exp i\left[n\left(\theta - \varphi_j + \frac{\pi}{2}\right) + \frac{2\pi lz}{c}\right]$$

$$\text{If } G_{nl}(R) = \sum_j f_j J_n(2\pi Rr_j)\exp i\left[-n\varphi_j + \frac{2\pi lz_j}{c}\right]$$

$$\text{then } F\left(R,\theta,\frac{l}{c}\right) = \sum G_{nl}(R)\exp in\left(\theta + \frac{\pi}{2}\right) \quad \cdots (47)$$

where Gnl is independant of θ.

To compare the calculated transform of a model with a diffraction pattern, it is necessary to evaluate the cylindrical average of the square of the Fourier transforms <FF*>. For semi-crystalline fibres the product of the lattice transform and the molecular transform on any layer line has the form

Gnl (R) exp in θ

$$\langle FF^* \rangle = Gnl(R)\,Gnl^*(R) \qquad (49)$$

Interpretation of Fibre Diagrams

We will describe the method for identifying geometrical parameters of the helix from its diffraction pattern, but only for a simple helix, i.e. one which repeats in one turn. The separation of the layer lines is inversely proportional to the pitch of the helix and the height of the first meridional intensity is inversely proportional to the vertical separation of the repeating atoms of the helix.

The position of the first maximum of each Bessel function on each layer line gives the helix radius. If the J4 term has a maximum at Rmax and from the Table of Bessel Functions the first max of $J_4(x)$ is at x = 5.3 then we can obtain the helix radius ro from

$2\, r_o\, Rmax = 5.3$

For more complex structures there may be contributions from a number of Bessel functions on a given layer line and the value of r_o need not be the same on all layer lines.

Nucleic Acids

Nucleic acids are long polymers made from nucleotides; there are three components in a nucleotide: a base, a sugar and a phosphate group. If the sugar is 2' - deoxy D - ribose the nucleic acid is DNA. There are four type of bases in DNA: adenine (A), guanine (G), cytosine (C) and thymine (T). A and G are purines and C and T are pyrimidines.

The phosphate group of one nucleotide is linked to the sugar of the next nucleotide, so the backbone of the polymer is a regular sequence of phosphate and sugar groups. The bases appear as side groups attached to the regular backbone. The order of the bases along the DNA determines which aminoacid is synthesized.

The major advance in obtaining reasonably good X-ray patterns from DNA came about in the early 1950's at the King's College Laboratories, mainly due to the efforts of M.F. Wilkins and Rosalind Franklin. They found that the control of humidity was very important in obtaining good patterns. using DNA stretched fibres of up to 100 μm in diameter they found that the structure changed from being highly crystalline (A form) at 75% relative humidity to semi-crystalline (B-form) at 92% relation humidity. One of the most important findings of this work was that the diffraction pattern was essentially the same from a number of different types of DNA indicating a base-independant regular structure. The B-form patterns indicated features due to a helical molecule, very similar to the model predicted by Watson and Crick. The reason for the sharp reflections in the A-form is that the DNA fibres are in a regular lattice; the reflections turn into arcs when the fibres are arranged irregularly giving poor orientation. A feature of both forms is the strong meridional reflection at 3.4Å spacing which shows that the vertical separation of the nucleotides 3.4Å. The separation of the layer lines gives the pitch of the helix, while the ratio of the pitch

to the vertical separation of the nucleotides gives the number of residues in one turn of the helix. In the A-form this number is 11 and for B form 10.

As mentioned above, the B-form shows more clearly the helical nature of the DNA molecule. The strong peaks along the layer lines give the radius of the molecule ; the strongest scattering is produced by the phosphate groups.

Design of Small Angle Scattering Cameras (i) X-ray Generation

The primary requisite of a small angle scattering (SAS) camera is an X-ray source. Until recently the only method of producing X-rays was by an X-ray tube consisting of a metal anode bombarded by electrons with sufficient energy. With the advent of synchrotron radiation a whole new field of activity has been opened up and its application to muscle research is described in Part 2.

The most popular anode target material used is copper which gives characteristic Kα-line at 1.54Å. Small angle scattering is proportional to $t \exp(-\mu t)$, where t is the thickness of the sample and μ the absorption coefficient; the expression is maximum at $t = 1/\mu$. For thicker samples there is more absorption, while thinner samples do not fully 'scatter'. For biological macromolecules in solution, the optimum thickness of the scattering material is about 1 mm.

The most commonly used source size (i.e. the size of the electron beam hitting the anode target) is 1 mm x 0.1 mm. The strength of the source is directly proportional to the electron beam current; the highest power X-ray generators require special cooling of the anodes and one method used is to construct the anode in the form of a large 'disc' and rotate it at high speed to spread the heat loading over a wide area. The most commonly used rotating anode generators have a power rating of 1 - 2.5 kW, 40 kV and 20 - 60 mA of electron beam.

(ii) Monochromatisation The X-rays emitted by the Cu target consist of the characteristic K and L lines super-imposed on a 'white' spectrum due to bremsstrahling. For most small angle scattering experiments it is necessary to monochromatise the beam i.e. to eliminate all but some unique wavelength - usually theCuKα line.

The linear absorption coefficient for elements show a sharp discontinuity at certain wavelengths related to their atomic number. Thus Nickel strongly absorbs Kβ but transmits Kα and is generally issued for eliminating the Kβ component and shorter wavelength white radiation.

A second method of monochromatisation which can also focus the beam involves total reflection from a smooth mirror. The angle of incidence has to be very small (a few mrad) for total reflection to take place; wavelength selection can then be made by adjusting the angle of incidence to only accept the Kα radiation and reject the Kβ and shorter wavelengths. Bending the mirror to the appropriate radius of curvature focuses the source at the detector and this can improve the 'resolution' of the camera.

Finally, one can combine a mirror with a crystal monochromator to obtain precise monochromatisation and this type of camera is discussed in the techniques section of muscle diffraction.

(iii)Collimation

Collimation is of vital importance in making accurate measurements because the signals i.e. the scattering produced by the sample, are very weak in comparison with the incident beam. If only a tiny fraction of the

direct beam is scattered from a poorly adjusted slit into the detector, it is enough to swamp the real 'signal'. As shown in the 'muscle' camera the important point is to have 'guard slits' to cut out parasitic scattering from the preceding slits but without impinging themself into the direct beam.

Solution Scattering Studies on Chromatin

One of the most fascinating problems in structural biology is that of packaging extremely long lengths of 1 to 2 metres of DNA into the tiny volumes (about 10 μm diameter) of the cell nucleus. Clearly several degrees of folding are required for 'storage' but it is also known that gene regions have to be unfolded and exposed. DNA is combined with a number of proteins, known as histones to form chromatin, from which chromosomes are made. Five types of histones are found in chromatin and the same histones are found in a wide range of enkaryotic cells indicating a high degree of conservation. Histones are positively charged and bind to DNA which has a number of exposed negative charges.

In dilute solutions of chromatin, assuming there is no interaction between molecules, it will be distributed at random. The scattering pattern then corresponds to the square of the Fourier transform of a single "super-helix".

The characteristic X-ray diffraction pattern consists of maxima at 110, 55 37 27 and 22Å and any model of chromatin structure has to explain this data. The first clue came from biochemical experiments with DNAse digestion which indicated regions of enhanced accesibility to nucleases the repeating unit being about 200 bp long. Soon after electron microscope studies showed globular particles 60-80Å wide connected by thin fibre. A model, proposed by Kornberg, suggested that 200 bp of DNA associated with 9 histone molecules comprising 2 each H4, H3 H2A and H2B to form 'beads'.

Small angle scattering measurements have produced shape and mass parameters for the nucleosome. With neutrons one can change the density of the solvent by introducing varying amounts of D_2O and H_2O and match out the protein or DNA component. They found that the radius of gyration for protein was 31Å and for the DNA 51Å indicating that the protein is on the inside and DNA on the outside.

The structure of the nucleosome has been determined to near-atomic resolution by crystallographic methods applied to three dimensional crystals of the nucleosomes.

Bibliography

C.R. Cantor and P.R. Shimmel, Biophysical Chemistry Part II, W.H. Freeman & Co. 1980.

K.C. Holmes and D.M. Blow, "The Use of X-ray Diffraction in the Study of Protein and Nucleic Acid Structure", Interscience Publishers 1965.

PART 2

X-ray Diffraction from Muscle

A.R. Faruqi

M.R.C. Laboratory of Molecular Biology

Hills Road

Cambridge CB2 2QH

United Kingdom

To be published in "Proceedings of the Eighth International Nathiagali Summer College on Physics and Contemporary Needs", Islamabad, Pakistan.

Contents

1. Introduction

Recent developments in modern biology have benefited enormously from a variety of physical techniques originally developed for use in physics. Notable examples are the use of electron and nuclear magnetic resonance, autoradiography, spectroscopy, electron microscopy and X-ray and neutron diffraction. In all these cases the ideas behind the techniques were developed by physicists and this was followed by applications in other disciplines. One of such techniques adapted for biological problems is that of X-ray diffraction; the successful application of this technique has been accompanied by an enormous increase in complexity and sophisitication to cope with the special nature of biological problems.

In a growing number of instances where proteins have been crystallized (into single crystals) the molecular structure has been solved to near atomic resolution. More recently, large structures such as viruses, have also been crystallised and the structure determined, though with somewhat lower resolution. It is still not possible to obtain crystals of even larger macro-molecular assemblies, found in the contractile part of striated muscle, but it is still possible to obtain very useful structural information on the ordered part of the structures with diffraction techniques. The general principles for the theory of this type of diffraction, known as fibre diffraction, were initially developed for the explanation of diffraction from helical structures like DNA but have found very important application in the interpretation of a whole range of fibrous proteins.

2. Muscle Structure: Brief Details

A very fundamental characteristic shared by all living creatures is that they can all move, due in all instances to the existence of some form of muscle system whose contraction results in the movement. Such a universal means of movement would in itself be an important enough reason for making a study of it's structure to understand the molecular mechanisms in operations, but there is another more fundamental reason for this study viz. that it is a remarkable piece of natural machinery designed to convert chemical energy dervied from food, into mechanical work in the form of movement. The main constituents of muscle are arranged with some degree of regularity, as discussed later, which enables one to use X-ray diffraction techniques to study the structure. Certain types of other biological systems, involved in movement, e.g. cytoplasmic streaming or flagellar movements are known to have similar proteins as in muscle and it is likely that a detailed understanding of the molecular mechanisms in muscle contraction will be of help in understanding these related phenomena as well. A large mass of information has been built up using vertebrate skeletal muscle, usually from frog, and in all our discussion we will use only this type of muscle to illustrate any results.

3. X-ray Diffraction from Muscle

A brief introduction to muscle structure is presented to illustrate how the X-ray pattern can be correlated with the structure at a macro-molecular level. Our view of the structure of muscle is based on a number of complementary techniques, but most importantly on X-ray diffraction and electron microscopy. Figure 1 shows schematically the more important structural features in striated muscle, based mainly on various types of electron microscopic observations[2]. The contractile proteins are contained in long thin myofibrils which are 1-2 μm in diameter; large numbers of myofibrils are packed together to form fibres. The most striking feature of the muscle is two types of filaments arranged in a periodic fashion along the muscle length. The basic unit of repeat, known as a sarcomere and is defined as the region between the Z-lines; in a resting muscle the sarcomere length is about 2.5 μm. The thin filaments, which are about 1000Å long and are 50-70Å in diameter, are attached to the Z-line. They consist mainly of a polymerised form of the protein actin (F-Actin) along with smaller quantities of some other proteins which have an important control function in the contraction mechanism. The thin filaments inter-digitate with the thick filaments which consist mainly of myosin. The thick filaments are about 1500Å in length and 100-120Å in diameter and have a periodic arrangement of 'projections' on their surface. As discussed later the projections form cross-bridges with thin filaments and play a vital role in contraction.

Considering the laterial arrangement of the filaments by taking a cross-section through the myofibrils, as shown in the lower part of Fig.1, it is striking how well-ordered the positions of the filaments are. The thick filaments are arranged on a hexagonal lattice with the thin filaments on the trigonal points. This type of arrangement gives rise to a well defined X-ray pattern along the equator which is informative regarding the relative distribution of mass between the two filaments.

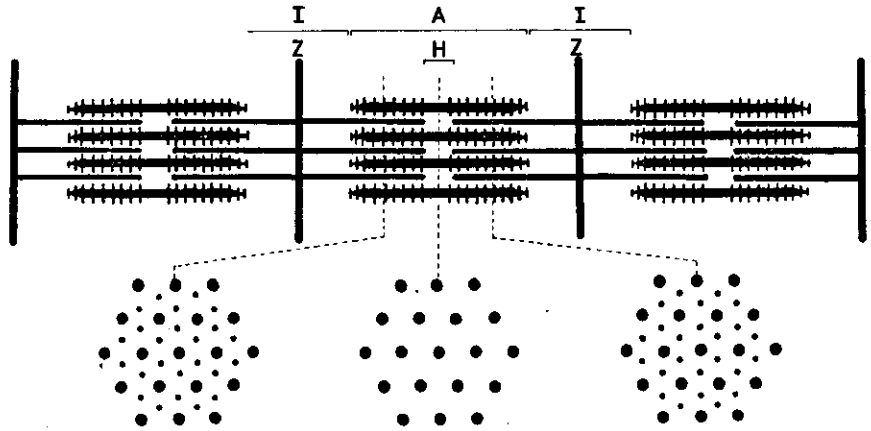

Fig.1 Schematic Diagram showing the lateral and cross-section view of the thick and thin filament organisation.

The main premise of muscle contraction is that the myosin projections are able to form cross-bridges with actin in the thin filaments and then go through some conformational change which produces a relative sliding motion between the thick and thin filaments[3,4]. A large number of cross-bridges, cycling asynchronously, generate the force which is transmitted through the thin filament and the Z-line to the ends of the muscle which is connected through tendons to the skeleton. The macroscopic movement of the skeleton is thus in response to the force generated by a very large number of cross-bridges located in a number of muscles.

The size of the cross-bridges ($\sim 10^2$ Å) and the speed with which they cycle ($\sim 10^{-3}$ sec) combine to make a detailed study of the cross-bridge cycling phenomena very difficult. One of the most fruitful techniques which has been applied to this problem is that of time-resolved X-ray diffraction from contracting muscle. The main advantage of X-ray diffraction is that one can study whole muscle in the natural living state and with synchrotron radiation cameras discussed later one can even achieve the necessary time resolution for making dynamic studies on certain regions of the X-ray pattern. The main disadvantage is that it only gives an average picture of the whole muscle and one cannot follow changes in individual molecules.

The periodic arrangement of thick and thin filaments in the contractile part of vertebrate muscle gives rise to a X-ray diffraction pattern which

can be reasonably correlated with the structure. A typical X-ray pattern from resting frog sartorius muscle taken on a synchrotron camera is shown in Fig. 2. The equatorial part of the pattern is believed to originate in the lateral packing of the thick and thin filaments, the position of the reflections being related (inversely) to the actual spacing of the filaments and the intensities to the amount of

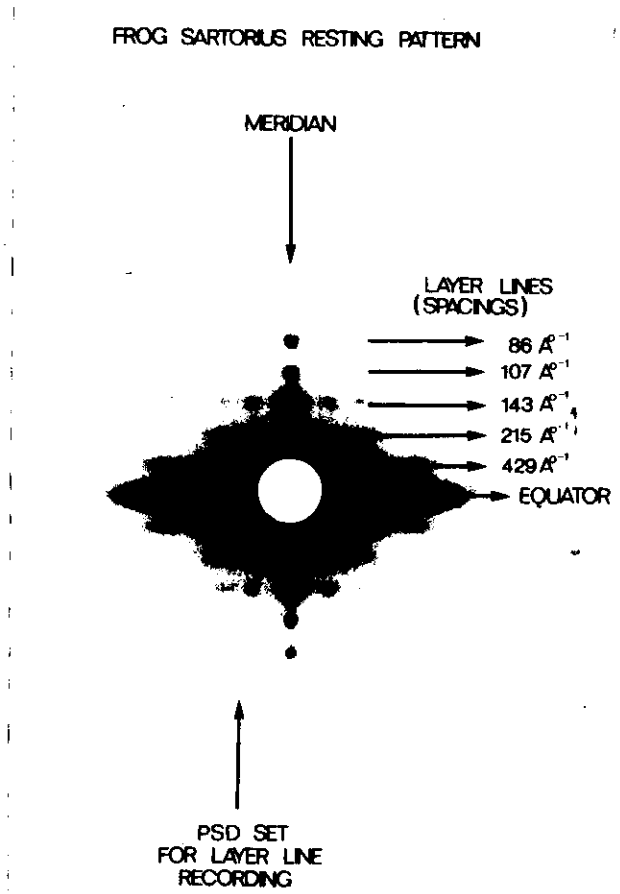

Fig.2 Small angle X-ray pattern from relaxed muscle showing strong scattering on the equator, meridian and myosin layer lines.

scattering matter within the unit cell. The inner reflection, indexed as (1,0), arises mainly from the thick filaments and the (1,1) from thick and thin filaments; Fig.3 shows a typical equatorial pattern recorded on a linear detector[21]. Early experiments[6] indicated that the intensity of the (1,0) was about twice as strong as the (1,1) in a resting muscle, but

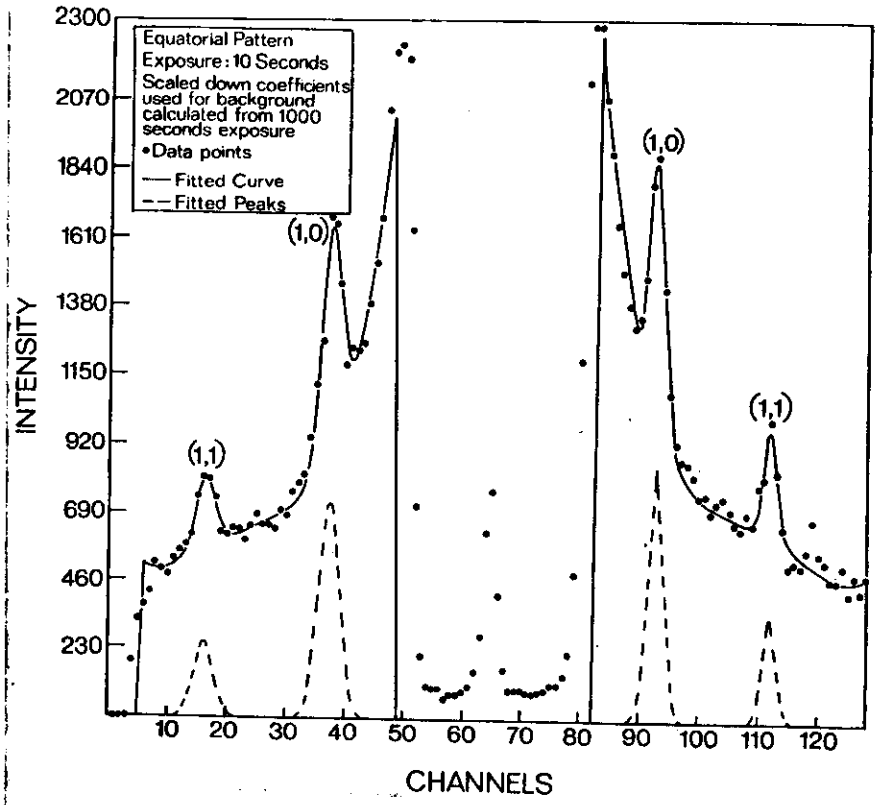

Fig.3 Equatorial pattern from relaxed muscle recorded on a linear position sensitive detector. The filled circles are data points and the solid line is a computed curve which assumes the peaks to be gaussion and the background as a 4th order polynomial.

during contraction there was a dramatic reversal of intensities: the (1,0) decreased by about a factor of 2 while the (1,1) increased by a factor of 2. This change was explained on the basis of a transfer of mass from near the thick to the thin filaments. As mentioned earlier, electron microscopic studies had already shown clear evidence of projections arranged regularly on the thick filaments; it was postulated (and has since been established) that during contraction, the projections extend out to the thin filament and form cross-bridges between the thick and thin filaments. The movement of the cross-bridges away from the region of the thick filaments represents the transfer of mass.

The myosin projections are arranged on an approximate helix on the surface of the thick filaments, three pairs of cross-bridges occurring every 143Å on a helical repeat of 429Å. This arrangement of cross-bridges gives

rise to characteristic layer lines expected in diffraction from helical structures with a spacing of 429Å and a strong meridional reflection at 143Å. The distribution of layer line intensities are given by the size and position of the cross-bridges; the further out the cross-bridges move the intensity peak moves 'inwards', i.e. towards the origin. If the regular helix is disrupted the layer line intensities are reduced.

There are additional layer lines in the X-ray pattern arising from the helical arrangement of actin monomers in the thin filaments but these are considerably weaker than the myosin layer lines and are not registered in the pattern shown in Fig.2. The thin filaments also contain additional proteins notably tropomyosin and troponin, which are important in the control of muscle contraction. The position of the former, viz. tropomyosin has a significant effect on the 2nd actin layer line. Using X-ray diffraction associated with the thin filaments, it was shown that in resting muscle tropomyosin prevents myosin heads from interacting with actin but during contraction it moves sufficiently to allow myosin-actin interaction to take place, leading to cross-bridge formation and force generation[8]. Discussion of this point is beyond the scope of this review though recent evidence from synchrotron radiation experiments give further support to this view as it is possible to study the detailed time course of the activation mechanism[9].

4. Time Resolved Measurements: Main Requirements.

As discussed above, X-ray patterns can be obtained from live muscle at rest and with some difficulty from contracting muscle as well; provided the recording of data could be speeded up this suggested a possible method for following dynamic changes in muscle structure at a molecular level during contraction. A number of separate technical developments were required for this objective to be achieved (if not completely, at least partly). Firstly, a large number of studies were carried out on resting and contracting muscle which helped to optimise the experimental procedures regarding the preparation of muscle specimen and keeping them alive and healthy over a large number of artificially induced contractions and exposure to X-rays. Secondly, much more intense source of X-rays were developed by using synchrotron radiation cameras instead of the conventional X-ray generator based cameras. Thirdly, the detection of the X-ray pattern, originally carried out on film was changed to position sensitive detectors with a reduction in exposure time. Fourthly, new methods of electronic data acquisition had to be developed which synchronized the data acquisition with the contraction cycle. Fifthly, new software was developed to deal effectively with the large amounts of data obtained.

In order to look at the problem of recording time resolved X-ray diffraction patterns in a little more detail, we discuss the general experimental strategy. The main requirements are on X-ray camera with suitable focusing optics optimised for muscle, geometry and a detector system for recording the diffraction pattern. For time resolved measurements it is essential to synchronize data acquisition precisely with the physiological condition of the muscle as shown in Fig.4. Normally the muscle is kept alive in a special solution with oxygen bubbling through and is forced to go through a series of contractions by applying electrical stimulii of the appropriate amplitude. The timing of the stimulii is derived from a master timing circuit which also controls data acquisition; the same timing is used for performing rapid length transients on the muscle.

The data rates on a laboratory based X-ray generator are sufficiently low not to cause saturation problems with conventional detectors. However, with the considerably more powerful synchrotron radiation sources the rate handling capabilities of the detectors are pushed to the limit. For instance, taking the equatorial (this contains about half of the rates in

SCHEMATIC DIAGRAM OF DATA COLLECTION SYSTEM FOR RECORDING TIME RESOLVED DIFFRACTION PATTERNS.

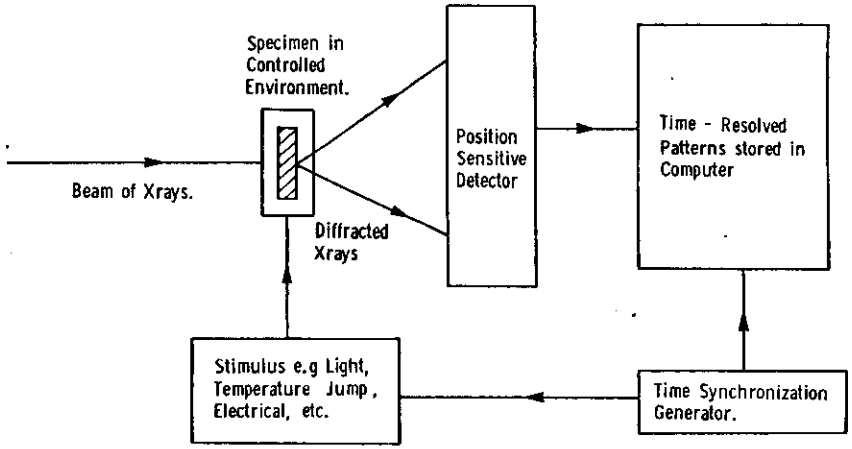

Fig.4 Schematic diagram showing the primary features of a system for making time resolved measurements.

the whole pattern) slice of data as an example, the data rates on a laboratory source are ∿ 10 kHz while on a synchrotron source they are 2 - 10 MHz, the latter being beyond the capabilities of conventional detectors. We have developed a new type of linear detector, the Multiwire Linear Detector, for coping with this situation[10,12,13,14]. The time resolution which is required is normally not a problem from a purely electronic point, being at its most demanding about 1 millisecond. A number of muscle parameters i.e. tension, length, etc also have to be recorded on the same time scale.

Early experiments used X-ray sensitive film as the medium for recording diffraction patterns, both from resting and contracting muscle. The time resolution of such measurements was limited to about 1 second, because it was necessary to use a shutter for cutting out X-ray beam for non-relevant periods of the contraction cycle. The situation was considerably improved with the introduction of the position sensitive detector with suitable electronics[16].

With the help of this technology one of the earliest findings was that during a twitch, the intensity change in the equatorial reflections preceded the tension development by about ∿ 10 ms. An illustration of this effect, but recorded very recently is shown in Fig.10. (we have chosen this recent experiment in order to illustrate the performance of the Multiwire Linear Detector). As expected, the (1,0) increases and the (1,1) decreases in intensity during the contraction but the change at half-maximum is ahead in time compared to the tension. This clearly indicates that structural changes occur as an essential pre-requisite to tension development. In a little more detail, it is postulated that the process of force generation goes through the following steps: the myosin heads make cross-bridges by attaching to the actin filament followed by a pause of about 10 ms when some structural re-arrangement may be taking place in the cross-bridge before the tension is generated.

5. Development of New X-ray Methods

It is clear that if one wishes to follow structural changes on a rapid time scale X-ray diffraction provides a very convenient tool for doing so. However, the more rapid the changes one wishes to follow, the shorter becomes the recording time available. As mentioned above, with modern electronic circuits it is simple to make the measuring time resolution as short as required but the limited intensity of the reflections pose a more fundamental limitation. To overcome this limitation, we and our colleagues in several laboratories have undertaken a long term program to develop high flux X-ray cameras based on synchrotron radiation.

5.1 Synchrotron Radiation

Electrons or positrons following a circular trajectory in a synchrotron emit synchrotron radiation, similar to radiation emitted by dipole oscillator, due to their acceleration towards the centre of the circle. In spectral terms the wavelength distribution of the emitted radiation resembles the radiation given off by a very hot black body (at a temperature of ∿ 10^7 °K) ranging from less than ∿ 1Å up to ∿ 1000Å with a peak in the region of 1-4Å depending the electron energy and the radius of curvature of the primary beam. The problems of converting this radiation into a useful tool for studying biological structures is in many ways different from the problems of setting up X-ray cameras on laboratory sources. The main geometrical difference is that the radiation emitted by the circulating electrons is strongly collimated in the forward direction (in fact the collimation is as good as that from lasers) whilst the radiation is isotropically emitted from conventional sources. The other main difference is that one gets a narrow wavelength spread in the emitted radiation from conventional sources whereas there is a continuum of wavelengths in synchrotron radiation.

The main requirement of the X-ray camera are to collect as large a flux as possible, to select a narrow waveband ($\delta\lambda/\lambda$) and to focus the primary beam. Several cameras have been designed for use on synchrotrons around the world posessing a number of common design features and we illustrate the design of such cameras with one of the earlier designs from our group[15] for use on the NINA synchrotron at Daresbury in the early seventies.

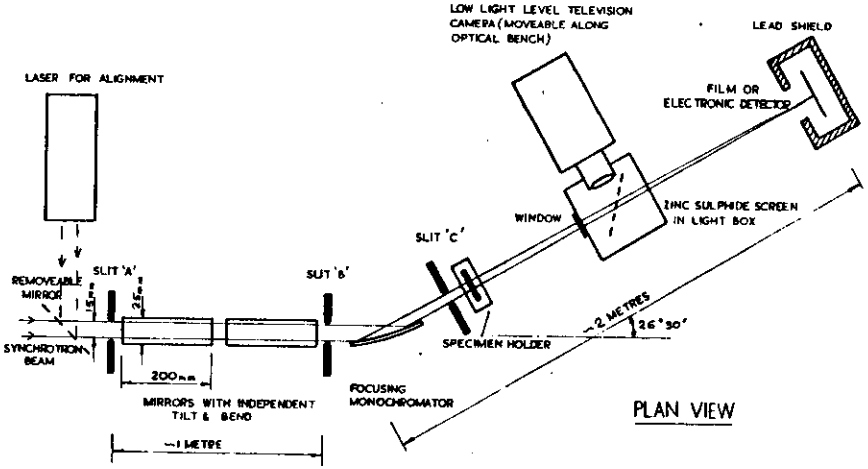

SCHEMATIC DIAGRAM OF LOW ANGLE X-RAY SCATTERING CAMERA FOR USE AT NINA

Fig.5. Schematic diagram showing the main components of a small angle X-ray camera using synchrotron radiation.

The first optical component in the camera, illustrated in Fig.5, are a pair of totally reflecting mirrors bent to the appropriate radius of curvature to focus the source (i.e. the cross-section of the electron beam) in the detector plane. The mirrors have a wavelength cut-off which removes wavelengths longer than some preset value depending on the angle of incidence of the primary beam. Focusing in the horizontal plane is achieved by a bent crystal monochromator usually made of Germanium which also selects a narrow waveband from the incident radiation.

To prevent stray radiation from entering the detector it is essential to have collimating slits which restrict the beam in both the vertical and horizontal direction. The last set of slits (Slit C in Fig.5) and the specimen are usually mounted on an optical bench, several metres long, aligned along the path of the monochromatised beam to enable smooth changes in specimen to detector distance.

The ambient radiation levels in the vicinity of the camera are usually too high for safe operation by manual control so it is necessary to build remote controls for all the optical components, specimen holder and detector. A closed circuit low light level television camera is used for initial setting up of the beam from a 'safe' area which also has the remote controls for the other components.

Gains or improvements in using synchrotron cameras over conventional ones vary with the nature of experiments but for typical experiments these are:

(i) an increase in useful X-ray flux by about a factor of 1000,

(ii) an improved signal-to-nose ratio due to the high degree of parallelism in the beam,

(iii) an ability to study patterns with much higher resolution (i.e. larger Bragg spacings) due to longer camera lengths and 'cleaner' cameras,

(iv) an ability to select wavelength used in a given experiment by choosing the appropriate Bragg angles in the monochromator crystal and perform wavelength scans over a range of wavelengths to study anamolous dispersion effects.

5.2 X-ray Detectors and Data Acquisition Systems

Recording X-ray diffraction patterns on film has the great advantage of being simple to use but for our experiments has the major drawback that it is very difficult to arrange for recording with any time resolution - particularly for times as short as a millisecond. Film also has an inherent 'fog' level which decreases the signal-to-noise ratio (by adding 'noise' over the whole area) hence requiring longer exposures to record signals with a given precision. This form of noise is almost totally absent in position sensitive detectors (PSDs) based on proportional counters. The other advantages in using position sensitive detectors are that the dynamic range of the measurements is much greater, limited only by the size of the memory and the efficency of detection is much higher than for film.

It is an interesting exercise to calculate the improvements in recording speeds, for particular types of X-ray patterns, when a position sensitive detector is used instead of film. The background noise or fog in film corresponds approximately to 0.1 O.D. Units which is equivalent to 10^6 blackened grains per 10 mm^2. An X-ray reflection, covering an area of 10 mm^2 area with 1000 photons/second would require 1 second of counting time to give a statistical accuracy of 3% in a position sensitive detector. In the film however, due to the 10^6 "counts" to start with, it would require 50 seconds to achieve a similar accuracy. In other words the PSD is faster by about 50 times for such reflection. If the X-ray reflection occupies a smaller area, but contains the same number of counts per second, the speed advantage is reduced while for larger areas it is greater. For typical muscle reflections and layer lines the speed advantage is in the range 10-100.

We have developed several types of position sensitive detectors and data acquisition systems for recording muscle data but we will restrict our discussions to only the more recent developments. We discuss two types of position sensitive detectors, one with fairly good spatial resolution but limited counting rate ability and a second one with very high counting rate capability but with somewhat poorer spatial resolution. Both detectors have selective advantages in specific experimental situations.

The first type of detector extracts spatial information with the help of an external delay line, illustrated schematically in Fig.6. The detector

consists of an anode plane sandwiched between two cathode planes, the sensitive volume being filled with a suitable gas mixture. If an incoming X-ray photon is absorbed in the gas one or more photoelectrons are emitted which accelerate in the electric field, towards the anode. The drifting electrons gain sufficient energy from the electric field to cause further ionisation resulting in an avalanche of electrons and positive ions, the electrons ending up on an anode wire. The positive ions drift away from the anode due to the electric field generating an induced charge on a number of cathode wires (or strips), the distribution of the induced charge being close to the position of the incident photon. The cathodes are coupled to an LC-delay line with suitable characteristics and the 'envelope' of the induced charge travels to either end of this delay line at a speed governed by the delay line properties. The difference in the arrival time of the pulses at the two ends gives the position of the incident X-ray photon.

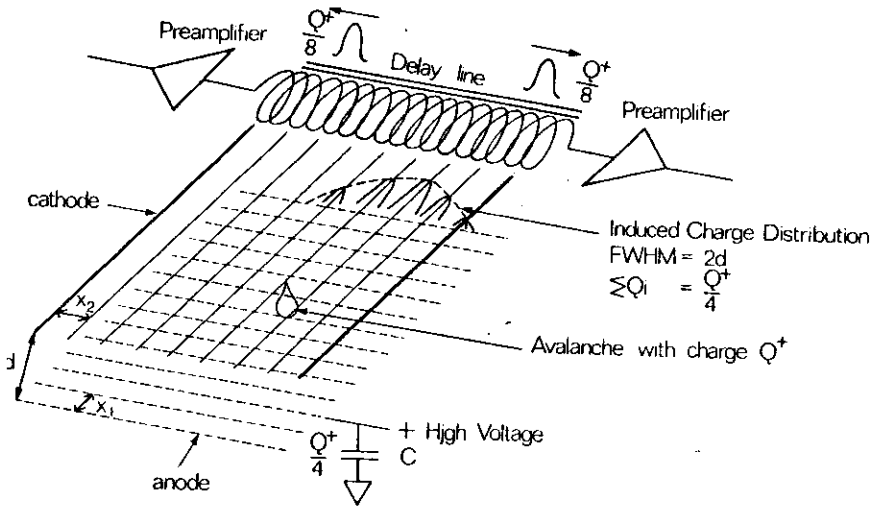

Fig.6 Principle of operation of a detector based on a delay line.

The electronics required for converting the timing pulses at the ends of the delay line in to a digital number, representing the position value, is simple in principle, but to obtain high spatial resolution or to enable high counting rates one requires more elaborate circuits. A typical system for recording X-ray patterns with the delay line detector is shown in Fig.7. The primary timing signals at both ends of the delay line are amplified and shaped in an amplifier with suitable time constants to give accurate timing information. In fact, the time of interest is the difference between the two signals, and this is obtained by using the earlier signal to start a Time-to-Digital Conversion stopped by the later signal. The digital value, representing the position is stored in a random access memory under the

control of a PDP 11/03 computer. This type of system is capable of handling rates upto 200 kHz and spatial resolution of ∿ 150 μm (fwhm), which allows data to be collected from most parts of the muscle pattern. More economical systems can be constructed by substituting an analog-to-digital converter for the time-to-digital converter and data stored in a multichannel analyzer; the main disadvantage being that it is slower by about a factor of 4.

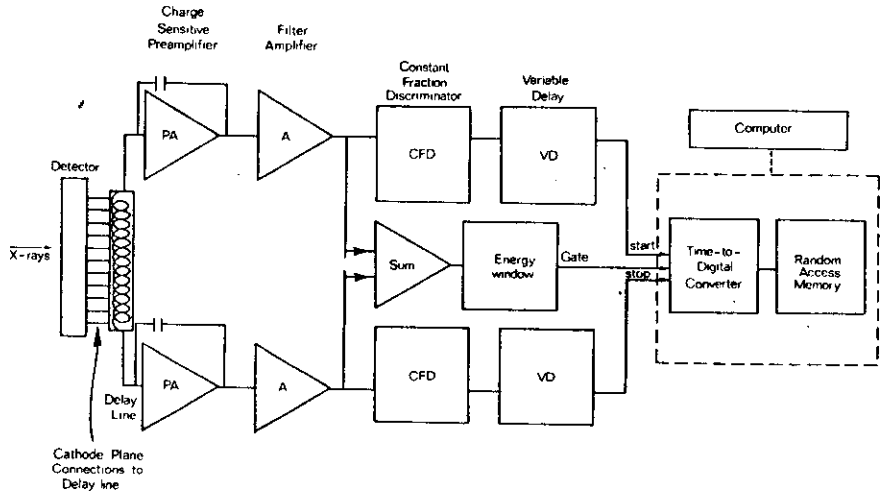

Fig.7. Block Diagram of electronics required for the delay line based position sensitive detector.

The second type of linear detector relies for its fast speed of operation on parallel readout of the anode wires, each of which is equipped with a complete readout channel as shown in Fig.8. The main limitation on counting rates in proportional counters is due to space charge saturation around the anode wire. A detector with 100 anode wires is thus able to count at approximately 100 times the speed of a detector with a single anode wire and rates in excess of 10 MHz over the whole detector are feasible. The spatial resolution in the MWLD is limited by the discrete character of the anode wires; if the anode wires have a 1 mm spacing then this represents the approximate spatial resolution. It is possible, however, to compute shifts in peak centroids to accuracies of better than 0.1 mm by using simple centre of gravity algorithms.

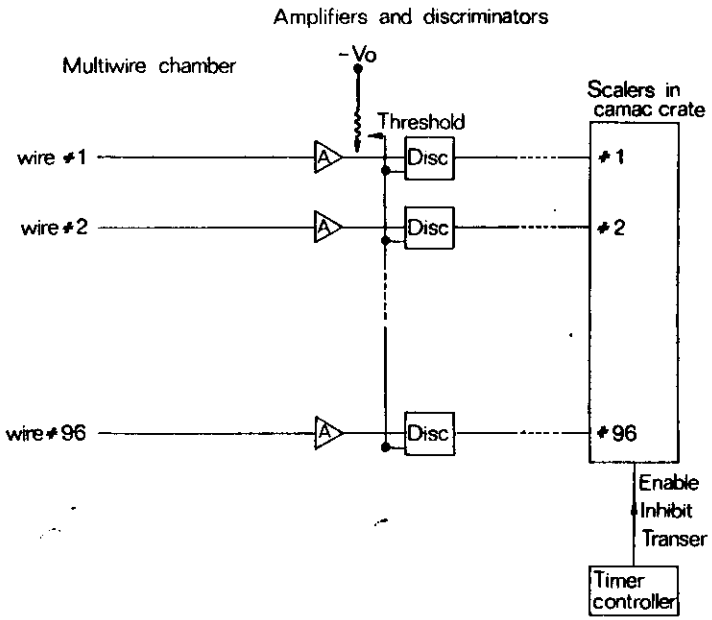

Fig.8. Operating principles of a parallel readout multiwire detector.

A typical system for making time resolved measurements on muscle is shown in Fig.9. The system was built for performing experiments using synchrotron radiation and shows the interface of the Multiwire Linear Detector and a number of other electronics circuits to a CAMAC dataway with an LSI 11/03 or 11/23 as a control computer[10,11,13]. The timing for the whole experiment is controlled by the Master Timer Controller in which these times are preset prior to the experiment. Timing for various functions is obtained from a 10 MHz quartz crystal oscillator after suitable scaling down. One of the timing functions is that very 30 seconds or so, it generates an electrical stimulus through a separate circuit and opens an X-ray shutter to allow X-rays to fall on the muscle specimen. The Timer also enables the scalers to count for the frame time period and then

transfers the data to a random access memory with the help of a special readout module. This process is repeated over the preset number of time frames. At the end it goes into a waiting mode while the software transfers data from the RAM to disc where it updates the previously stored patterns in the correct sequence. Typically, one can have upto 256 frames of data with 3 different frame times. When the preset number of cycles have been completed, the program writes a header section with the experimental details.

The system has been tested at the SRS, Daresbury and muscle equatorial data obtained on the small angle beam line. A typical (1,0) time course during an isometric twitch along with tension are shown in Fig.10 by way of illustration. The experiment shows the 10 ms time lag in the tension compared to the intensity change as mentioned in Section 3. 6.

6. Recent Results

During the past six years or so we have been collecting time resolved data under various conditions at the EMBL Outstation using the DORIS Storage Ring in Hamburg, FRG. The results of these experiments have been published in a series of papers from which just two types of experiments have been chosen to illustrate the results in outline [18,20,23]. In the first type of experiment the muscle is kept at a constant length during the contraction; this is known as an isometric contraction. In the second type of experiments a rapid length change is imposed on a contracting muscle. In either case the parameters of interest are the intensities of various reflections and how they vary on a rapid time scale. In some cases the spacings of reflections are of interest as well as the width of the reflection.

6.1 Results on Isometric Contraction

The behaviour of the myosin based layer lines and the meridional reflection during isometric contraction have been studied in some detail making use of high intensity synchrotron cameras[18]. One of the advantages of the reduction in exposure time compared to conventional cameras, is that it is possible to do complete experiments on freshly dissected muscle specimen. This is a great improvement over laboratory experiments some of which had to be carried out over periods of days to obtain adequate intensities. Even with such long exposures it is not possible to record the weaker parts of the pattern. Moreover, as the data on contracting muscle has to be integrated over a large number of twitches, the muscle fatigues and one gets inaccurate results.

The interpretation of data can only be carried out after suitable data reduction, involving background stripping, peak fitting, etc. From the earliest experiments, one of the most striking results obtained was on the variation of the myosin based off-meridional layes line during isometric contraction which showed a dramatic decrease in the intensity at the onset of contraction. Although the layer line intensities decrease during contraction it is informative to show relative changes in intensity to compare with rise in tension at the onset of contraction. We will only discuss the behaviour of the 429Å layer line which is the most intense but secondary layer lines at 215Å, 143Å, 106Å and 86Å also show similar decreases in intensity though the magnitude of the changes are somewhat smaller[18].

The time course of the 429Å layer line intensity on a relative scale is shown in Fig.11 along with tension development and they both appear to be very similar. When one studies the changes in some detail, it appears that the intensity changes are ahead of tension by about 10 ms, when the specimen is at 10°C. During the decay of tension the 429Å intensity recovers on a similar time scale to the tension. In short, the layer line intensities seem to accurately mirror the rise and decay of tension. Similar behaviour is observed at different temperatures, the time scales getting slowed down at lower temperatures.

The changes in the 143Å meridional reflection during an isometric contraction are very different from the layer lines. A detailed study has been made of a number of meridional reflections but we will only discuss the behaviour of the 143Å and more briefly the 215Å reflections. At the onset of contraction indicated by the rise in tension, there is a sharp drop in intensity of the 143Å reflection but this is soon reversed and the intensity increases to a value which is similar to the resting value and in some cases even higher (Fig.12). This is followed by a substantial decrease in intensity as the tension recovers back to the resting value. Another interesting change observed in this reflection is that the width of the 143Å reflection across the meridian nearly doubles during contraction and the time course of this change is as shown in Fig.13. The width of the reflection reflects the inherent disorder in the primary scattering units, namely the cross-bridges, and an increase in the width arises from increased disorder during contraction. Interestingly the width or disorder increases in phase with tension but remains high even when the tension has decayed to resting value. Due to the width increase the measured intensity is lower than the 'real' intensity and when this correction is made, it is seen that the 143Å intensity increases by about 50% above the resting value during a contraction and that it decreases down to the resting value in phase with tension. The width decreases back to the resting value but with a delay of several hundred milliseconds after the tension has decreased, leading to the apparent dramatic drop in intensity as the tension drops[18].

The meridional reflection on the second layer line (215Å) has a different time course from the 143Å meridional as shown in Fig.14. The behaviour is very similar to that of the 429Å layer line, following the tension closely.

The interpretation of the layer line and meridional changes are described in some detail in a recent paper[18] and we only summarise them here. As mentioned earlier, the layer lines are generated by the helical ordering of cross-bridges on the thick filament in a relaxed muscle. During contraction the helical symmetry is disrupted, as cross-bridges go through the attachment-detachment cycle, with consequent loss of the layer line intensity. The magnitude of the intensity change gives us some idea about the fraction of cross-bridges which are disrupted during contraction and the time course of the changes tells us the speed at which this disruption occurs. The 143Å meridional reflection arises from the axial repeat of the cross-bridges which probably improves during contraction, probably due to attachment of the distal end of the cross-bridge to the thin filament preventing movement of the cross-bridge.

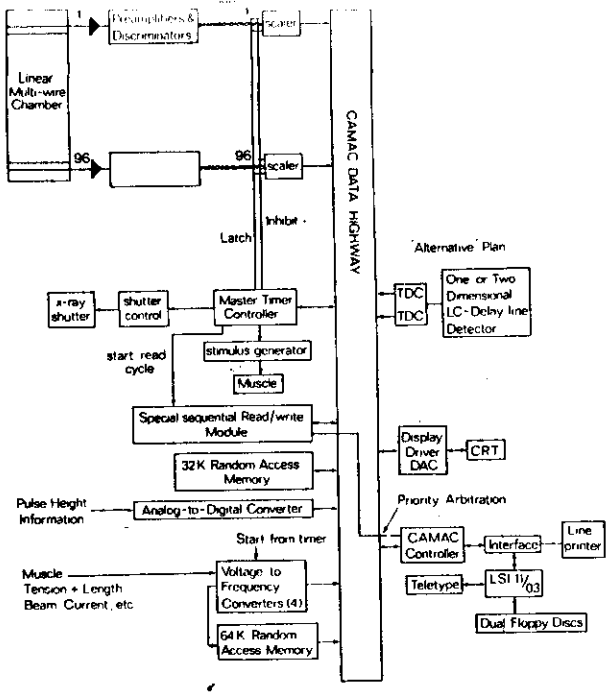

Fig.9 Block Diagram showing complete data acquisition system

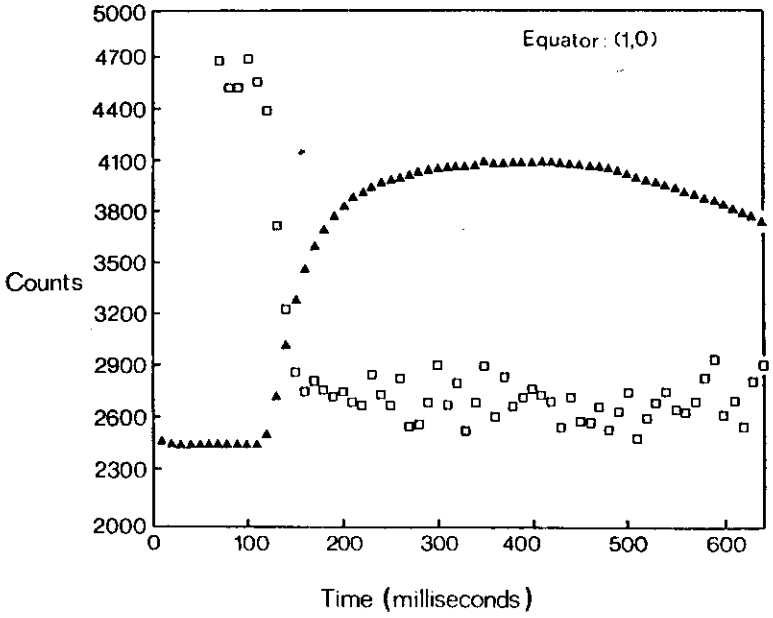

Fig.10. Time course of the (1,0) equatorial reflection during an isometric twitch. Data recorded on a Multiwire Linear Detector at the SRS, Daresbury.

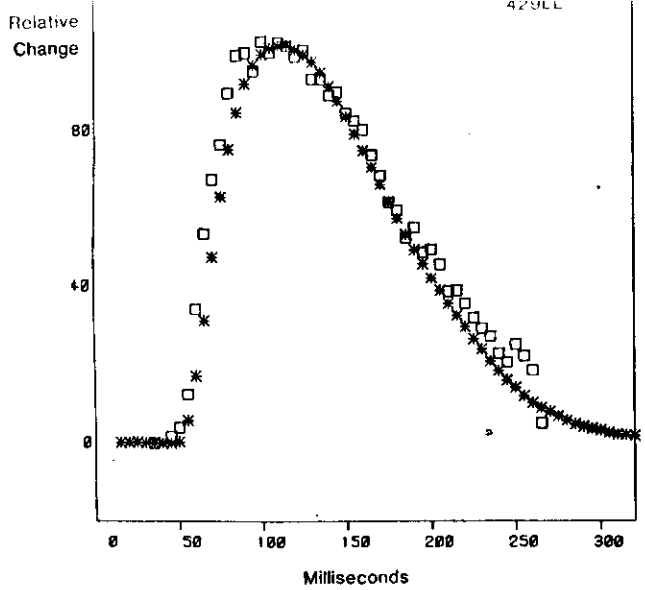

Fig.11. Time course of the 429Å layer line intensity during an isometric twitch. Changes are shown on a relative scale. Squares refer to intensity and stars to tension. Time scale is given on the horizontal axis.

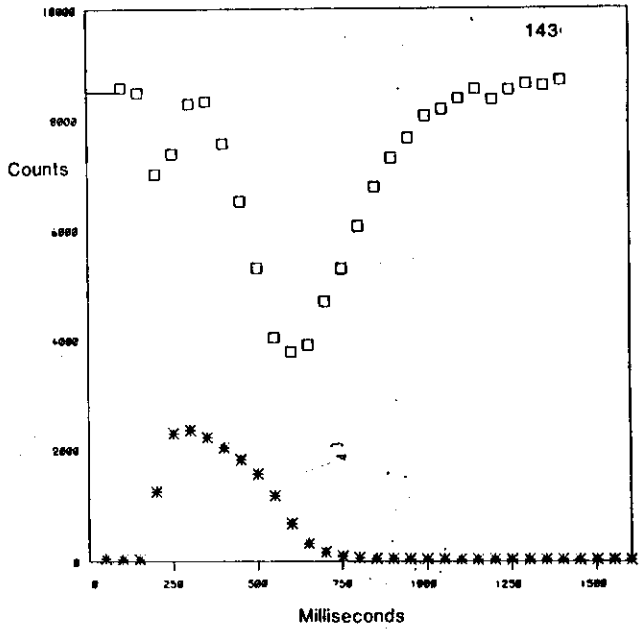

Fig.12 Time course of 143Å intensity during an isometric twitch. Each time frame is 50 milliseconds square refer to intensity.

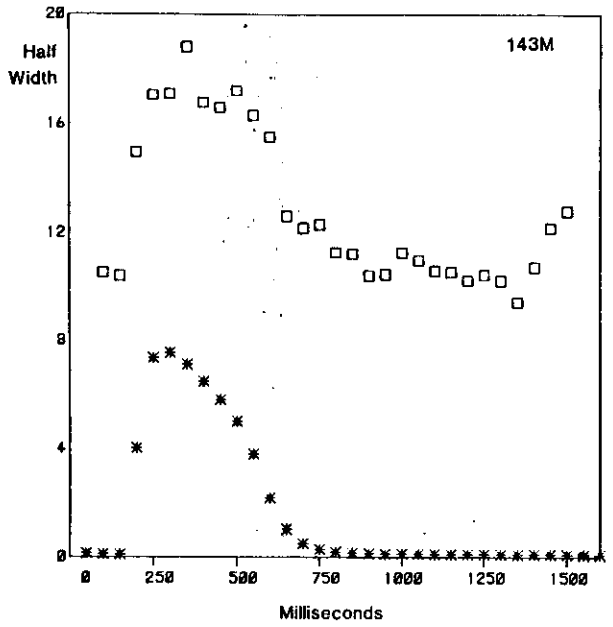

Fig.13 Width changes in the 143Å reflection during an isometric twitch. Same time scale as in Fig.12 squares refer to width.

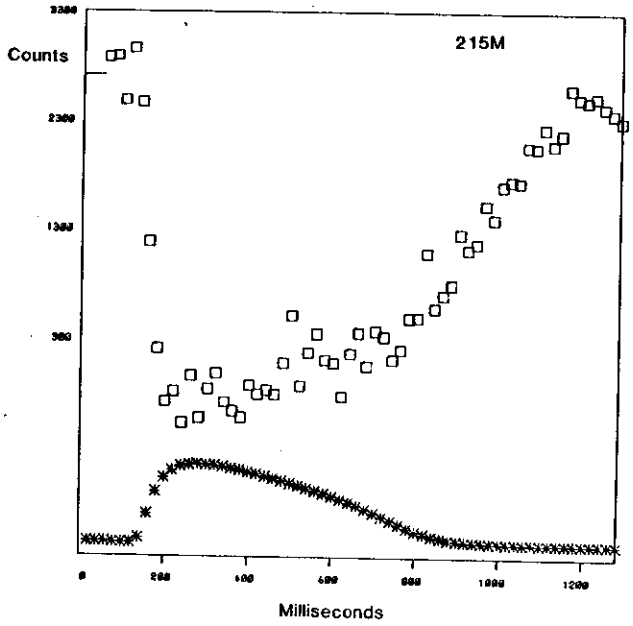

Fig.14 Time course of the 215Å meridional reflection during isometric contraction.

6.2 Measurements with Rapid Length Changes

One way of attempting to synchronize the orientation of the cross-bridges is to change the length of a contracting muscle by a small amount (∿ 100 Å) which brings them to the end of their working stroke. The technical difficulty of such measurements is that the length change has to be completed in a time scale which is short compared with the cross-bridge cycle, preferably shorter than 1 millisecond [19,20]. A large number of experiments have been performed to determine the effect of such rapid length changes on various parts of the muscle pattern. The most interesting of the intensity changes appear to occur in the 143Å meridional reflection. The time course of the 143Å intensity during a quick release, in which the muscle is shortened by about 1.5% of its length is shown in Fig.15. As mentioned above the length change is imposed on a contracting muscle so we are only looking at the intensity and tension during the 'plateau' of contraction. The tension drops simultaneously with the length change, because the cross-bridges go 'slack' as the filaments slide in the same direction as the cross-bridge 'push' recovering with a time constant of about 20 ms. The intensity of the 143Å meridional reflection shows three phases: an almost instantaneous drop in intensity with tension (there is in fact a time lag of about 0.7 ms) to ∿ 30% of the starting value followed by a recovery with a fast time constant (∿ 5ms) and then a slower one (∿ 20 ms). Similar experiments can be performed by applying a quick stretch to the contracting muscle instead of a release. In such experiments it is found that the 143Å intensity drops with tension but the recovery shows only the longer time constant, as shown in Fig.16.

A very interesting result is obtained by combining two length transients, a quick release followed a few milliseconds later by a quick stretch, both of the same magnitude.

The first step produces the expected drop in intensity but if the following step is made within, say, 2 ms, the intensity recovers almost back to its pre-release level as shown in Fig.17. However, if the stretch is applied only 20 ms later, there is another drop in intensity similar to that observed in the first release. If the first step is a stretch and the second one a release then a similar result is obtained, i.e. a drop in intensity at the first step which recovers at the second step, provided there is only a short interval between the two steps. This time can be much longer than in the release-stretch case; if, however, it is as long as 45 ms, as shown in Fig.18, there is a drop in intensity at the second step as well. The conclusions of these experiments are that the rapid length changes are not merely introducing disorder in the filaments but producing a reversible structural change which causes the sharp drop in intensity and which in the subsequent step can be reversed. This is a striking confirmation of the original hypothesis that cross-bridges are actually made between the thick and thin filaments, something for which direct evidence had been lacking previously.

Experiments involving rapid length changes have also been carried out on other regions of the pattern, viz the equator, the myosin layer lines, the other meridional reflections and the actin reflections. The main feature of these experiments is that the intensity changes in response to rapid length changes are very small, particularly when compared to the changes in the 143Å meridional reflection discussed earlier. A full discussion of these experiments and their interpretation is given by Huxley, et al [20].

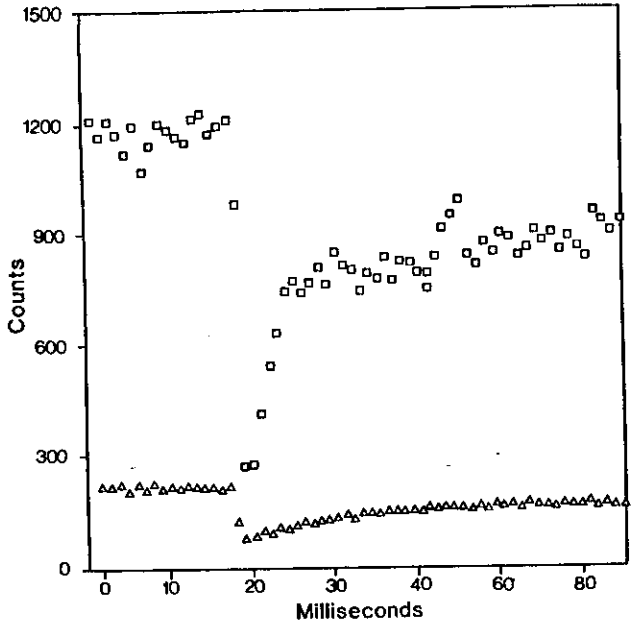

Fig.15. Record of the 143Å meridional instensity during a quick release. The intensity is shown as squares and the tension as traingles.

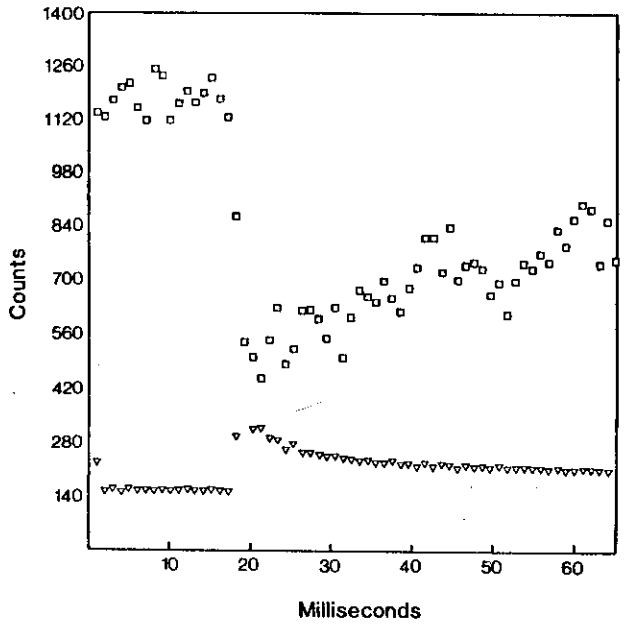

Fig.16 Record of the 143Å meridional intensity during a quick stretch.

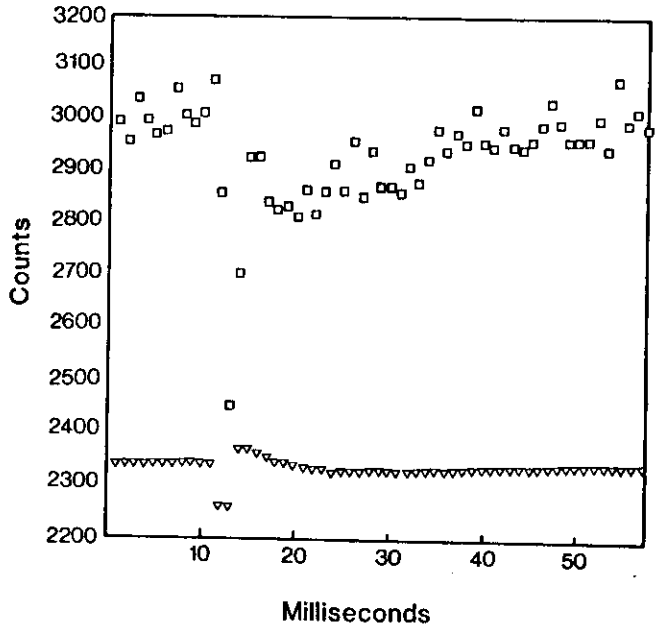

Fig.17. Effect of a release followed 2 milliseconds later by a stretch on

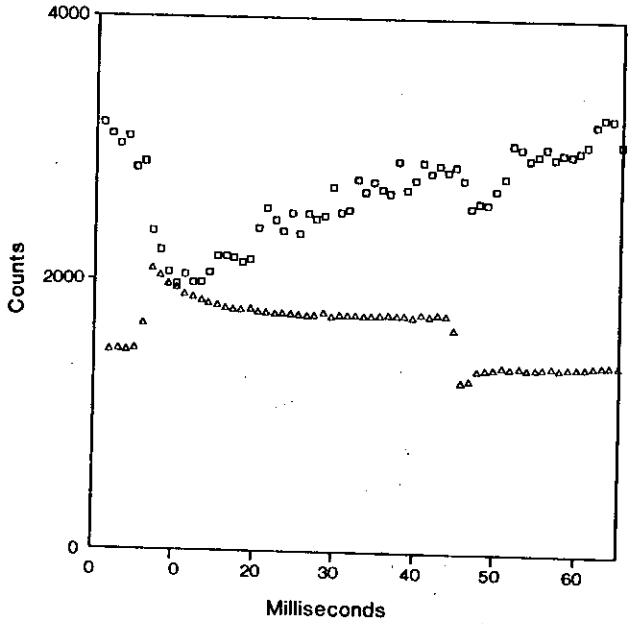

Fig.18 Stretch followed 45 milliseconds later by a release on the 143Å intensity.

7. Conclusions

The understanding of the detailed molecular mechanism operating in muscle during contraction and consequent force generation has been significantly enhanced by a combination of several new X-ray techniques. The application of synchrotron radiation and fast position sensitive detectors allow measurements to be made on a time scale close to the biochemical rate constants operating in muscle.

The results presented in this paper can only represent the beginning of a whole new series of experiments which are taking place now and will continue into the future to unravel in greater detail the mysteries of muscle contraction and allied phenomena.

References

1. Biophysical Chemistry Part II: Techniques for the study of biological structure and function. C.R. Cantor and P.R. Schimmel. W.H. Freeman & Co. (1980).
2. H.E. Huxley, The Structure and Function of Muscle 301-387 (1972). Ed. Bourne. Academic Press.
3. H.E. Huxley, Science, 164, 1356-1366 (1969).
4. H.E. Huxley, Proc. Roy. Soc. London Ser. B., 178, 131-149, (1971).
5. H.E. Huxley and A.R. Faruqi, Ann. Rev. Biophys. Bioeng. 12 (1983) 381. This is a general review paper dealing with Time-Resolved X-ray Diffraction from Muscle and contains a fairly complete bibliography up to mid-1982.
6. H.E. Huxley, J. Mol. Biol. 37 (1968) 507.
7. J.M. Squire, 1981. The Structural Basis of Muscular Contraction, Plenum Press.
8. H.E. Huxley, Cold Spring Harbour Symp. Quant. Biol. 37, 361 (1973).
9. H.E. Huxley, M. Kress and A.R. Faruqi, Biophys. Journal, 45, 10a (1984).
10. A.R. Faruqi, H.E. Huxley in Proc. Taniguchi Symp., Tsukuba, 367-401 (1978).
11. A.R. Faruqi, H.E. Huxley, in Scattering Techniques Applied to Supramolecular and Non-equilibrium Systems, ed. S-H Chen, B. Chu, R. Nossal, pp.201-27. Plenum.
12. A.R. Faruqi and C.C. Bond, Nucl. Instr. and Meth. 176 (1980) 71.
13. A.R. Faruqi and C.C. Bond, Nucl. Instr. and Meth. 201 (1982) 125.
14. A.R. Faruqi, IEEE Trans. Nucl. Sci. NS-30 (1983) 358.
15. J.C. Haselgrove, A.R. Faruqi, H.E. Huxley & U.W. Arndt, J. Phys. E., (Sci. Instr.), 10, 1035-1044 (1977).
16. A.R. Faruqi, IEEE Trans. Nucl. Sci. NS-22, 2066-2073 (1975).
17. A.R. Faruqi, Nucl. Instr. and Meth. 217, 19-29 (1983).
18. H.E. Huxley, A.R. Faruqi, M. Kress, J. Bordas. M.H.J. Koch, J. Mol. Biol. 158, 637-84.
19. H.E. Huxley, R.M. Simmons, A.R. Faruqi, M. Kress, J. Bordas and M.H.J. Koch, Proc. Natl. Acad. Sci. USA. 78 (1981) 2297.
20. H.E. Huxley, R.M. Simmons, A.R. Faruqi, M. Kress, J. Bordas and M.H.J. Koch, J. Mol. Biol 169, 469-506, (1983).
21. A.R. Faruqi and H.E. Huxley, J. Appl. Crystallogr. 11, 449-454 (1978).
22. H.E. Huxley, Acta. Anat. Nippon 50, 301-325 (1975)
23. H.E. Huxley, A. R. Faruqi, J. Bordas, M.H.J. Koch, J.R. Milch, Nature 284:140-43.